# Locking of southward extrusion in favour of rapid crustal-scale buckling of the Greater Himalayan sequence, Nar valley, central Nepal

L. GODIN[1], T. P. GLEESON[2], M. P. SEARLE[3], T. D. ULLRICH[4] & R. R. PARRISH[5]

[1]*Department of Geological Sciences and Geological Engineering, Queen's University, Kingston, Ontario, K7L 3N6 Canada (e-mail: godin@geol.queensu.ca)*

[2]*Department of Civil Engineering, Queen's University, Kingston, Ontario, K7L 3N6, Canada*

[3]*Department of Earth Sciences, Oxford University, Parks Road, Oxford, OX1 3PR, UK*

[4]*Pacific Centre for Isotopic and Geochemical Research, Department of Earth and Ocean Sciences, University of British Columbia, Vancouver, British Columbia, V6T 1Z4, Canada*

[5]*NERC Isotope Geosciences Laboratory, Keyworth, Nottingham, NG12 5GG, UK*

**Abstract:** The South Tibetan detachment system (STDS) bounds the upper limit of the Greater Himalayan sequence (GHS), which consists of the exhumed middle crust of the Himalaya. In the Annapurna range of central Nepal, the GHS comprises a sequence of amphibolite-grade augen gneisses with a 3.5 km thick leucogranite at the higher structural levels (Manaslu granite). Two major low-angle normal-sense shear zones have been mapped. The Chame detachment has similar grade metamorphic rocks above and below and is interpreted as a ductile shear zone wholly within the GHS. The Phu detachment is a ductile–brittle normal fault which wraps around the top of the Manaslu leucogranite and defines the uppermost, youngest strand of the STDS, placing folded unmetamorphosed Palaeozoic rocks of the Tethyan sedimentary sequence above the GHS. Our data indicate that ductile flow and southward extrusion of the GHS terminated with cessation of movement on the brittle upper strand of the Phu detachment at *c*. 19 Ma, which was followed almost immediately by crustal-scale buckling. Argon thermochronology reveals that the bulk of the metamorphic rocks and lower portions of the Tethyan sedimentary sequence in the Nar valley cooled through the hornblende, biotite and muscovite closure temperatures at *c*. 16 Ma, suggesting very rapid cooling rates. The thermochronology results indicate that this cooling occurred 2–3 million years earlier than in the frontal part of the extruded GHS. Although the extrusion in the frontal part of the GHS must have locked at the same time as in the Nar valley, the exhumation there was slower, and most probably only assisted by erosion, rather than by rapid folding as is the case in the Nar valley. This buckling indicates a step northward in deformation within the Himalayan belt, which may be a response to a lower deforming taper geometry in the foreland.

Since the first orogen-parallel synconvergent normal faults were recognized in the Himalayas (Caby *et al.* 1983; Burg, 1983; Burchfiel & Royden 1985), there have been numerous studies attempting to understand the mechanics of normal faults which are synchronous and parallel with structurally lower thrust faults (e.g. Hodges *et al.* 1992; Searle *et al.* 1997, 2003; Vannay & Grasemann 2001). In the Miocene, two major parallel yet opposite-sense shear zones, namely the Main Central thrust (MCT), and the South Tibetan detachment system (STDS), were active and broadly coeval (Hubbard & Harrison 1989; Searle & Rex 1989; Hodges *et al.* 1992, 1996; Godin *et al.* 2006). However, both the MCT and STDS zones display complex multiple strands that might have operated at different times and under different mechanical conditions (plastic to brittle). For example, the MCT zone is often subdivided into a younger, structurally lower brittle thrust, and an older, structurally higher ductile shear zone (e.g. Arita 1983; review in Godin *et al.* 2006). The present-day position of the Greater Himalayan sequence, the exhumed metamorphic core of the Himalaya, is interpreted to have resulted from predominantly ductile extrusion of mid-crustal material between these two opposite-sense shear zones. Several extrusion mechanisms have been proposed, ranging from wedge-type geometries (Grujic *et al.* 1996; Grasemann *et al.* 1999),

*From*: LAW, R. D., SEARLE, M. P. & GODIN, L. (eds) *Channel Flow, Ductile Extrusion and Exhumation in Continental Collision Zones*. Geological Society, London, Special Publications, **268**, 269–292.
0305-8719/06/$15.00 

to general shear distributed throughout the Greater Himalayan sequence (Vannay & Grasemann 2001), to channel flow within the core of the Greater Himalayan sequence (Beaumont *et al.* 2001, 2004; Grujic *et al.* 2002).

The STDS marks the structural and metamorphic upper limit of the Greater Himalayan sequence, separating 'unmetamorphosed to weakly metamorphosed [folded] strata of the hanging wall (Tethyan sedimentary sequence) from upper-amphibolite facies gneisses and leucogranites of the Greater Himalayan sequence footwall' (Hodges 2000, p. 338). It is a system of ductile shear zones and brittle normal faults recording a complex strain history. In various regions of the Himalayan orogen, it has been proposed that the STDS may have had an early thrust component (Weismayr & Grasemann 2002), overprinted by several phases of normal- and thrust-sense motion (Godin *et al.* 1999), and possibly also by dextral strike-slip motion (Pêcher 1991). More recently, Yin (2003) suggested that the STDS may represent a passive roof thrust within the MCT system. Certainly, there is general agreement that the fault system acted as a major ductile top-to-the-north normal-sense fault in the Miocene, coeval to the structurally lower MCT (Vannay & Hodges 1996; Godin *et al.* 2001; Godin *et al.* 2006), although some would argue that there is no evidence for synchronous motion (Murphy & Harrison 1999).

The portion of the STDS history coupled with the MCT, that we term the MCT–STDS coupling period, has led many to believe that the metamorphic core in the High Himalaya was extruded southward from its mid-crustal depths between these two kinematically and dynamically linked opposite-sense faults (Burchfiel & Royden 1985; Hodges *et al.* 1992; Royden 1996; Grujic *et al.* 1996, 2002; Beaumont *et al.* 2001). Both fault systems may have had, prior to or after the extrusive phase of the Greater Himalayan sequence, periods of independent motion, such as renewed late brittle (normal and/or thrust) reactivation, which are not associated with extrusion of the Greater Himalayan sequence. Structural, physiographic and geochronological data suggest segments of the MCT and STDS may have been active after the MCT–STDS coupling period (Harrison *et al.* 1997; Hurtado *et al.* 2001; Catlos *et al.* 2002). Nevertheless, although both structures may have been reactivated in recent times, these reactivations may be local and sporadic, without a dynamic coeval link between the two fault systems.

Central Nepal (Fig. 1a) is an ideal region to study the metamorphic core and its bounding structures. The area has a long history of geological investigations (Bordet *et al.* 1971; Pêcher 1975; Colchen *et al.* 1981). Furthermore, the Greater Himalayan sequence in the Annapurna range is exposed in two contrasting structural settings: in the well-studied 'frontal' north-dipping homoclinal slab (Le Fort *et al.* 1986; Hodges *et al.* 1996; Vannay & Hodges 1996; Godin *et al.* 2001), and in the structural windows provided by apparent domes north of the Annapurna range (Bordet *et al.* 1975; Le Fort *et al.* 1999; Godin 2001; Gleeson & Godin 2006). These two contrasting, yet spatially close, settings provide the opportunity to study and compare exhumation processes at various structural positions within the Greater Himalayan sequence.

The objectives of this paper are to present structural and geochronological constraints on the timing of cooling of the folded Greater Himalayan sequence exposed north of the Annapurna range in the Nar valley, and to compare the geometry and cooling ages from the Nar valley with previously published results from the Greater Himalayan sequence of the frontal homoclinal segment in the Kali Gandaki valley (e.g. Vannay & Hodges 1996; Godin *et al.* 2001). The ultimate goal of the paper is to document the geometry and timing of cessation of the MCT–STDS coupling, and make suggestions as to why this might have happened.

## Geology of north-central Nepal

The geology of north-central Nepal (Fig. 1a) is defined by three main lithotectonic units broadly striking east–west. The northernmost unit is the Tethyan sedimentary sequence, consisting of a *c.* 12 km thick passive margin succession deposited on the northern margin of the palaeo-Indian continent. In central Nepal, these sedimentary rocks range in age from Ordovician to Lower Cretaceous (Bordet *et al.* 1975; Colchen *et al.* 1981; Gradstein *et al.* 1992; Garzanti 1999). The lowermost Tethyan sedimentary sequence is metamorphosed to zeolite–lowest greenschist grade with a foliation typically defined by muscovite. The metamorphic grade decreases upwards to the epizone–anchizone boundary (Garzanti *et al.* 1994). The Tethyan sedimentary sequence is in normal fault contact with the underlying Greater Himalayan sequence along the Miocene-age STDS (Burchfiel *et al.* 1992). In central Nepal, the STDS includes the structurally lower ductile level of the Annapurna detachment zone (Brown & Nazarchuk 1993; Godin *et al.* 1999), which correlates with the Deurali detachment in the Annapurna Sanctuary (Hodges *et al.* 1996), and with the Chame detachment in the Marsyandi valley (Coleman 1996). The structurally higher

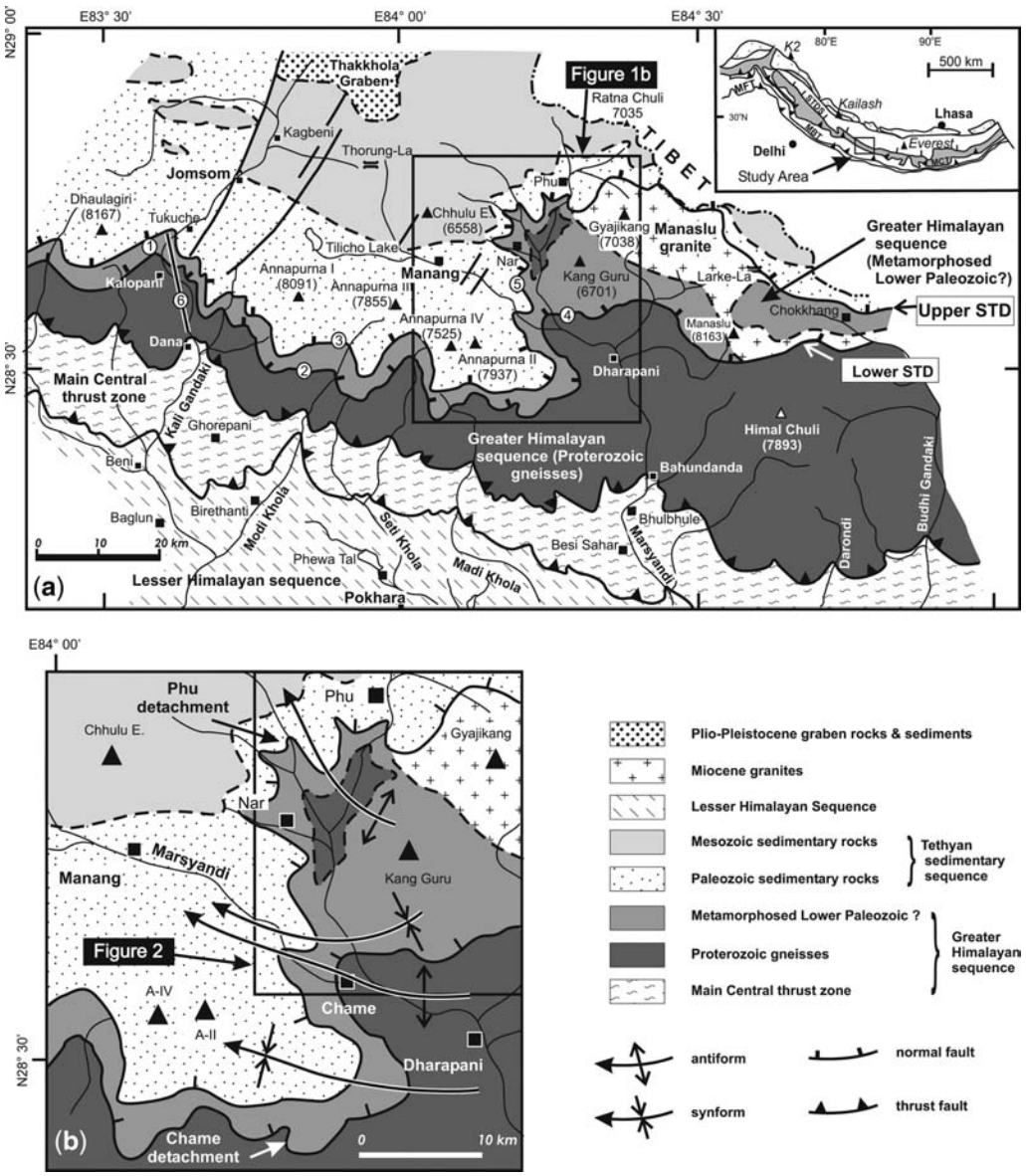


**Fig. 1.** (**a**) Regional geology map modified from Colchen *et al.* (1981) and Searle & Godin (2003). Inset shows the study area within the Himalayan orogen. Greater Himalayan sequence in grey; important structures noted are Main Frontal thrust (MFT), Main Boundary thrust (MBT), Main Central thrust (MCT), and South Tibetan detachment system (STDS). The various strands of the STDS are indicated by numbers. 1, Annapurna detachment; 2, Deurali detachment; 3, Macchapuchare detachment; 4, Chame detachment; 5, Phu detachment. Section line 6, indicates the study area of Vannay & Hodges (1996) and Godin *et al.* (2001) in the Kali Gandaki valley. (**b**) Map of Manang region, Marsyandi valley, showing area mapped in detail (box outline) and axial surface traces of the fold system affecting the Greater Himalayan sequence.

brittle level of the Annapurna detachment coincides with the Machapuchare detachment in the Annapurna Sanctuary (Hodges *et al.* 1996), and with the Phu detachment in the Marsyandi–Nar region (Searle & Godin 2003). Most of the surface trace of the STDS is exposed south of the Annapurna range (Fig. 1a). However, just east of Annapurna II, the fault system takes on a northerly

trend, wraps around the Miocene Manaslu leucogranite, and then resumes its easterly course (Fig. 1a, b). This change in orientation is due to a series of upright, shallow, west-plunging folds which, combined with topography, account for these two apparent orthogonal bends (Bordet *et al.* 1975; Searle & Godin 2003). In the Marsyandi valley, the STDS consists of two detachment faults (Fig. 1b): the lower ductile Chame detachment (Coleman 1996), and the upper ductile–brittle Phu detachment (Searle & Godin 2003). The Greater Himalayan sequence, representing the exhumed metamorphic core of the Himalaya, is located in the footwall of the STDS. It consists of amphibolite-facies Proterozoic gneisses intensely affected by Oligocene and Miocene thermal events (Coleman 1996; Vannay & Hodges 1996; Godin *et al.* 2001). The structurally lowest part of the Greater Himalayan sequence is in thrust contact with the Lesser Himalayan sequence along the north-dipping, south-vergent Miocene-age MCT zone (Bouchez & Pêcher 1976; Brunel 1986). The metasedimentary rocks in the immediate hanging wall of the Chame detachment were initially assigned to the Cambro-Ordovician levels of the Tethyan sedimentary sequence (Bordet *et al.* 1971, 1975; Colchen *et al.* 1981, 1986). Although this stratigraphic correlation may prove to be correct, their metamorphic degree (amphibolite facies) and highly sheared structural style suggest these rocks share a common tectonic history with the Greater Himalayan sequence (Searle & Godin 2003; Gleeson & Godin 2006).

## Geology of the Nar valley

### *Greater Himalayan sequence*

The Greater Himalayan sequence is typically described in terms of three distinct units, Unit I, Unit II and Unit III (Formations I, II, III of Bordet *et al.* 1971). The structurally lowest unit (Unit I), located in the hanging wall of the MCT, is dominated by a pelitic kyanite–sillimanite–garnet–biotite schist. The central and upper parts of the Greater Himalayan sequence are dominated by a hornblende–biotite gneiss (Unit II), 'interlayered' with a distinctive Lower Ordovician granitic augen gneiss (Unit III; Bordet *et al.* 1975; Colchen *et al.* 1981). Recent work in the upper part of the Greater Himalayan sequence in the Nar valley reveals a more complex lithological sequence with significant previously unrecognized marble and pelite layers, metamorphosed to amphibolite facies (Searle & Godin 2003; Gleeson & Godin 2006).

In the Nar valley, the Greater Himalayan sequence is separated into two distinct structural levels. The structurally lower level (Level 1), cropping out in the core of the Chako antiform along the Phu Khola (Figs 2 & 3), comprises hornblende–biotite gneiss (calc-silicate gneiss of Bordet *et al.* 1971), and a thin (50 m thick) sheet of highly strained biotite schist (*schiste à plaquette* of Bordet *et al.* 1971). Locally, this unit contains lenses of granitic augen gneiss that are interpreted to represent lower strained equivalents of the biotite schist. These two lower level units are correlated with Unit II and Unit III, exposed further south in the Marsyandi valley (Searle & Godin 2003; Gleeson & Godin 2006).

The rocks of the upper level (Level 2) consist of a biotite-bearing marble (Unit IV) and a garnet-bearing pelitic schist (Unit V). Petrography and garnet–biotite thermometry of the pelitic schist indicate peak metamorphic temperatures of 500–650°C, consistent with amphibolite-facies metamorphism (Gleeson & Godin 2006). These two upper level units are interpreted as previously undescribed components of the Greater Himalayan sequence, found structurally above the Chame detachment (Searle & Godin 2003; Gleeson & Godin 2006).

The Manaslu leucogranite forms in its eastern portion a 3 km thick sill of tourmaline–muscovite leucogranite located along the top of the Greater Himalayan sequence beneath the Phu detachment (Searle & Godin 2003). It is a peraluminous granite with extremely high Sr initial ratios, and is interpreted as a crustal minimum-melt granite derived from a protolith source similar to the sillimanite gneiss of Unit 1 (Le Fort 1981; Vidal *et al.* 1982). Earlier workers described the Manaslu leucogranite as intruding across the STDS into unmetamorphosed sediments of the Tethyan sedimentary sequence (e.g. Le Fort 1975, 1981; Colchen *et al.* 1986; Guillot *et al.* 1993). However, pressure–temperature conditions of rocks along the Nar valley and the upper Marysandi valley show that the carbonate rocks in which the leucogranite was intruded are at high metamorphic grade and do not exhibit contact metamorphic relations (Schneider & Masch 1993). Searle & Godin (2003) mapped a new upper strand of the STDS, called the Phu detachment, wrapping around the top of the Manaslu leucogranite; they place the Manaslu leucogranite wholly in the Greater Himalayan sequence, in common with all other Himalayan leucogranites. The Th–Pb ion microprobe ages of monazites from the Manaslu leucogranite define two major pulses of magmatism at $22.9 \pm 0.6$ Ma and $19.3 \pm 0.3$ Ma (Harrison *et al.* 1999). Structural studies along the Pangre glacier show that the Phu detachment cuts the contact of the Manaslu granite with the overlying Greater Himalayan sequence rocks (Fig. 2),

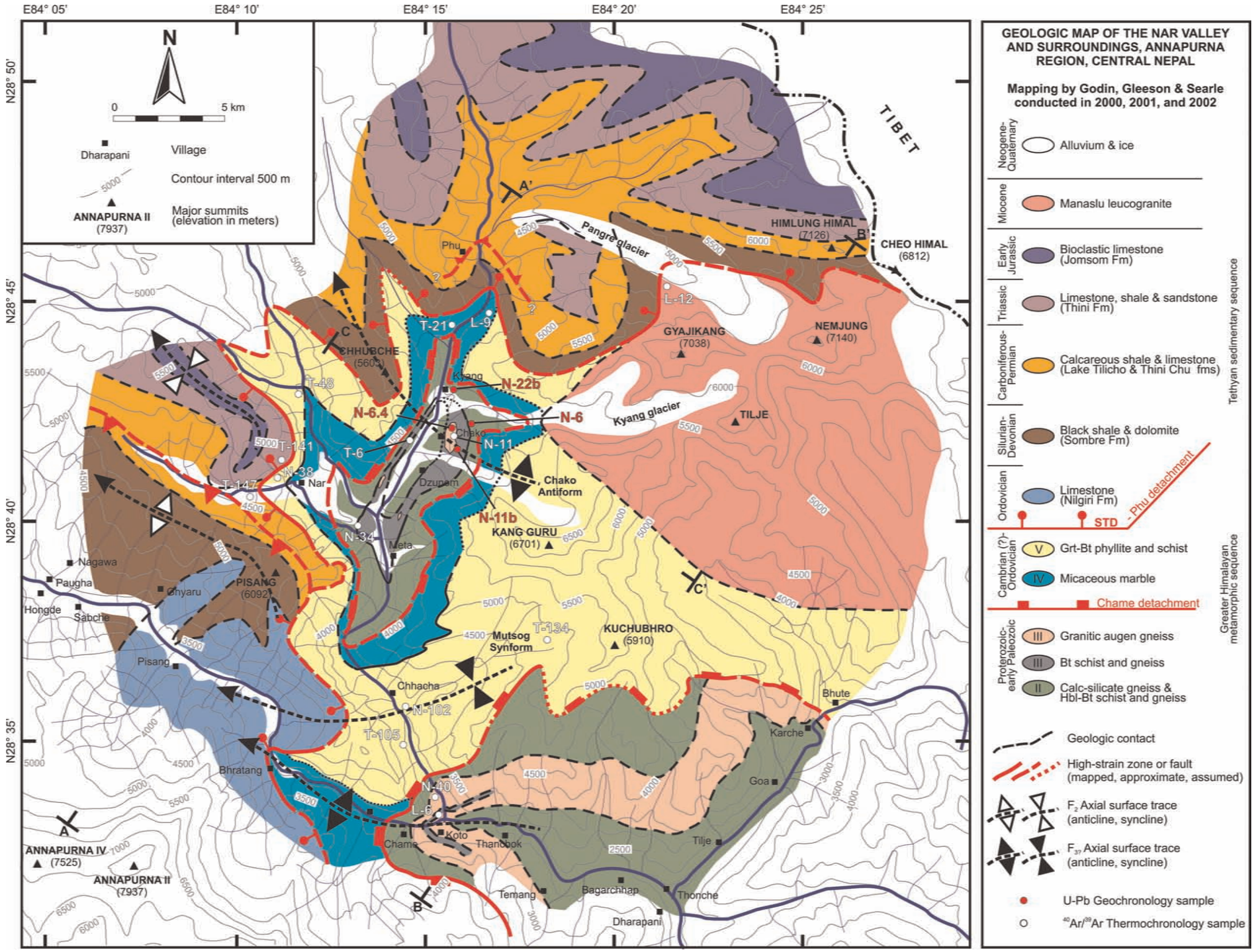


**Fig. 2.** Detailed geological map of the Nar valley, largely based on mapping in 2000, 2001 and 2002 by the authors. Detailed geology of the Tethyan sedimentary sequence is modified from Bordet *et al.* (1975), Fuchs *et al.* (1988, 1999), Coleman (1996) and Le Fort *et al.* (1999).

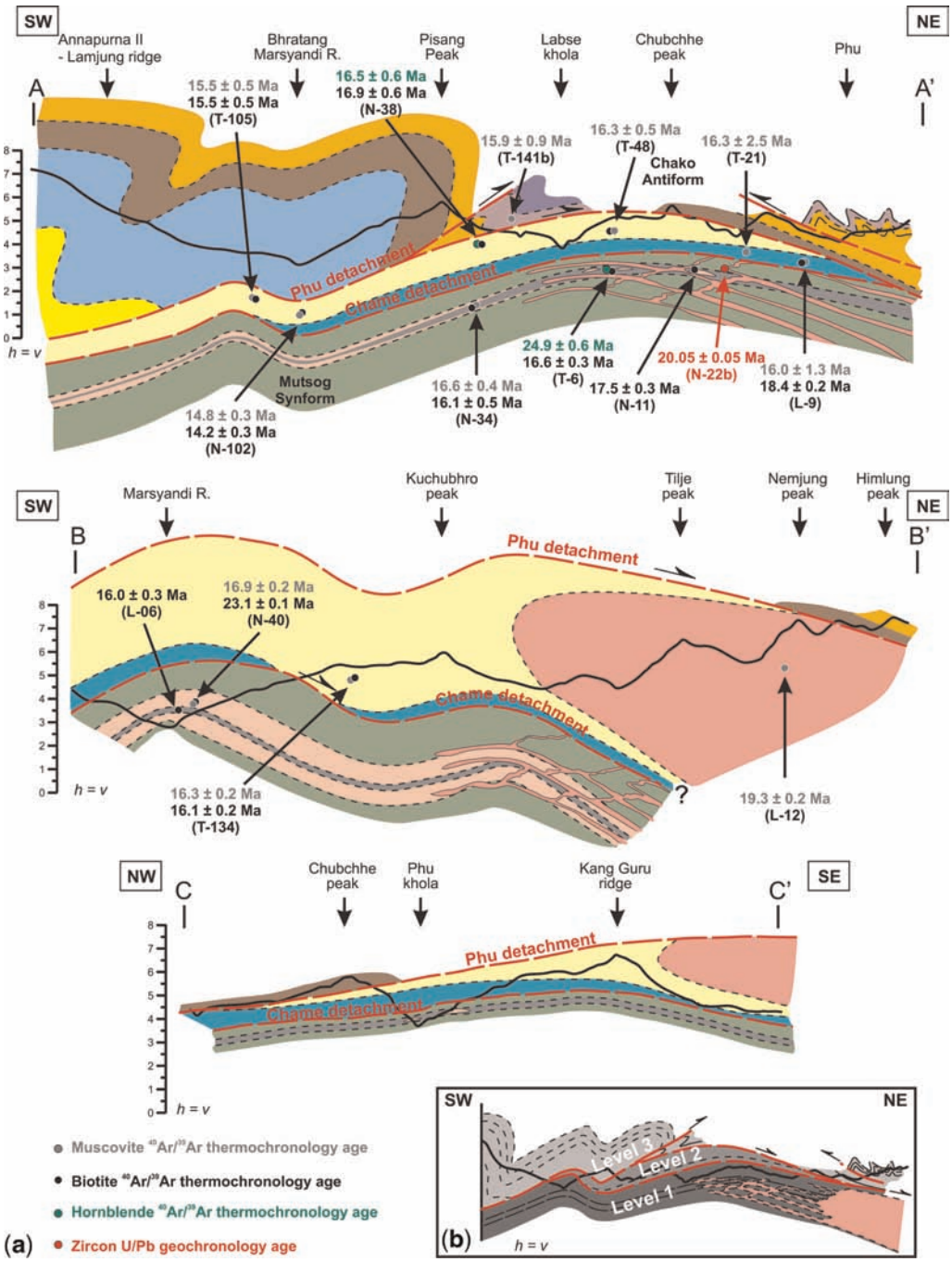


**Fig. 3.** (**a**) Two SW–NE geological cross-sections (A–A′ and B–B′), and one NW–SE cross-section (C–C′) in the Nar valley, showing distribution of results obtained from the $^{40}Ar/^{39}Ar$ thermochronology and U–Pb geochronology study. The section lines and legend are indicated on Figure 2. Modified from Searle & Godin (2003). (**b**) Schematic illustration of field area divided into three distinct structural levels: the Chame detachment separates the lowest structural level (Level 1) from Level 2; the Phu detachment separates Level 2 from the highest structural level (Level 3).

locally placing Tethyan sedimentary rocks in fault contact directly above the Manaslu leucogranite. The Phu detachment therefore must have been active after 19 Ma (Searle & Godin 2003).

### *Tethyan sedimentary sequence*

As indicated on the map (Fig. 2) and cross-sections (Fig. 3a), the distribution of the Tethyan sedimentary sequence (Level 3) in the Nar valley is confined to two regions. The southern region encompasses exposures near Nar village and Pisang Peak, whereas the northern region includes exposures near Phu village and Pangre glacier. These two regions are separated by the Chako antiform, which exposes metamorphic rocks of the Greater Himalayan sequence.

The Ordovician Nilgiri Formation, exposed in the Marsyandi valley near Britang and on the southern slopes of Pisang, is the lowest exposed stratigraphic level of the Tethyan sedimentary sequence. It consists of micritic grey massive to metre-thick beds of limestone, with rare poorly preserved brachiopods and crinoids, grading upwards into calcareous shale and siltstone (Bordet *et al.* 1975). The Nilgiri Formation is overlain by a Siluro-Devonian *Tentaculite*-bearing black shale and siltstone unit (Bordet *et al.* 1975), exposed on the northern flank of Pisang, and also in the immediate hanging wall of the Phu detachment in the Phu Khola, south of Phu village (Fig. 2). Brachiopod-rich Carboniferous–Permian calcareous shale and limestone of the Lake Tilicho and Thini Chu formations cap the Siluro-Devonian shale, and pass upwards into >200 m thick, black to grey Triassic limestone, shale and sandstone of the Thini Formation, visible in the vicinity of Nar and Phu villages (Fig. 2; Colchen *et al.* 1986). The uppermost stratigraphic unit exposed in the Nar valley is the Upper Triassic–Lower Jurassic Jomsom Formation (or Kioto Limestone; Garzanti 1999), consisting of a *c.* 500 m thick, grey to dun micritic limestone (Colchen *et al.* 1986).

## Structural constraints

Figure 3a presents two *c.* 35 km long NE–SW cross-sections of the Nar valley (A–A′ and B–B′), from the northern slope of Annapurna IV to north of Phu village and the Manaslu leucogranite, respectively. Both sections are linked by a third orthogonal NW–SE cross-section (C–C′). The field area is divided into three distinct structural levels, separated by two segments of the STDS (Fig. 3b): the two lower levels (Levels 1 and 2) are within the Greater Himalayan sequence, whereas the upper level (Level 3) is confined to the Tethyan sedimentary sequence. Rocks of Levels 1 and 2 are characterized by top-to-the-south ductile flow structures, locally concentrated into several metre-thick high-strain zones, in contrast with the polyphase-folding style preserved in the overlying Tethyan sedimentary sequence of Level 3. The Chame detachment (Coleman 1996) juxtaposes rocks of similar metamorphic grade (Schneider & Masch 1993), and is interpreted as a ductile top-to-the-north shear zone wholly within the Greater Himalayan sequence, separating Levels 1 and 2 (Searle & Godin 2003). The Phu detachment is a ductile–brittle top-to-the-north normal fault that defines the uppermost, youngest strand of the STDS, separating Level 2 from Level 3. The Phu detachment is folded into a series of open structures (Mutsog synform, Chako antiform; Figs 3a & 4a). Above Nar village on the south limb of the Chako antiform, the fault juxtaposes unmetamorphosed Palaeozoic rocks of the Tethyan sedimentary sequence (Level 3) above biotite marble (Unit IV) and garnet schist (Unit V) of the Greater Himalayan sequence (Fig. 4b). Further north, on the north-dipping limb of the Chako antiform, the detachment juxtaposes unmetamorphosed upper Palaeozoic and lower Mesozoic rocks of the Tethyan sedimentary sequence (Level 3) in its hanging wall against the Manaslu leucogranite (Level 2) in its footwall (Figs 2, 3a & 4c; Searle & Godin 2003).

### *Structural Level 1*

The structurally lowest level (Level 1) is composed of hornblende–biotite gneiss, leucogranitic augen gneisses and biotite schist, metamorphosed to amphibolite facies (up to 750°C; Schneider & Masch 1993; Vannay & Hodges 1996). These units constitute the footwall of the Chame detachment. Rocks within structural Level 1 are characterized by strongly developed continuous metamorphic foliation and ductile transposition fabrics, locally affected by south-verging folds. Quartz ribbons, mineral aggregate lineations, and a higher concentration of top-to-the-south shear-sense indicators are observed within 1- to 100-m-thick high-strain zones (Fig. 5a, b, c). Top-to-the-south shear-sense indicators include sigma porphyroblasts, C-S fabrics, C′ shear bands, and systematic north-dipping subgrain boundaries developed in quartz ribbons within Unit III granitic augen gneiss (Fig. 5b, c). Between high-strain zones, the rocks exhibit anastomosing fabrics, and lack mineral lineations and shear-sense indicators (Gleeson & Godin 2006). The upper boundary of Level 1 is defined by the top-to-the-north Chame detachment (Coleman 1996; Searle & Godin 2003).

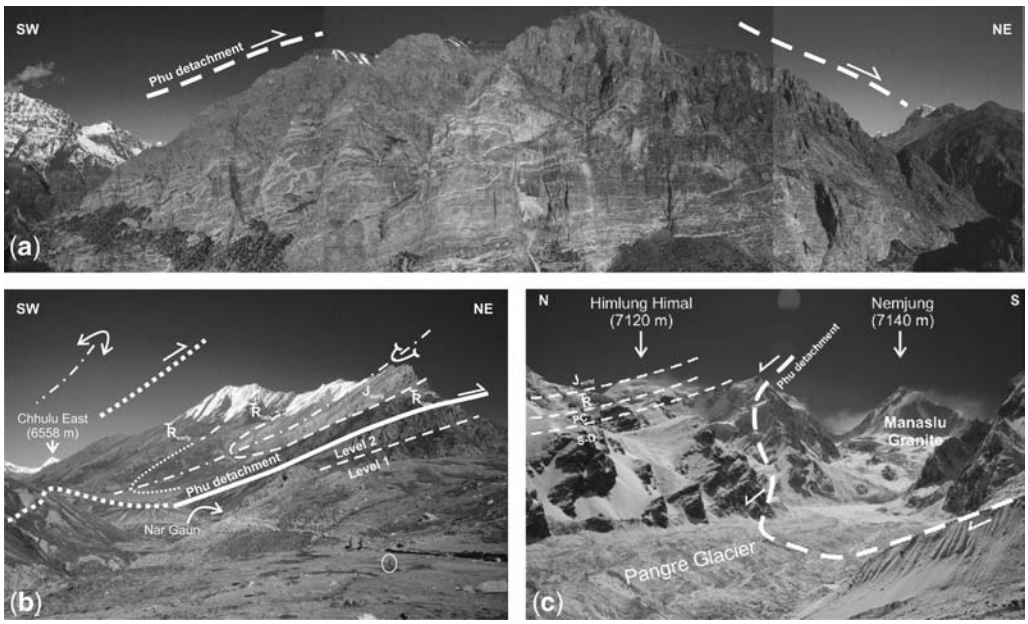


**Fig. 4.** Field photographs of the Phu detachment and immediate footwall rocks. This fault crops out in the Marsyandi valley near Britang, dips west around Pisang peak, dips south over the village of Nar, wraps over the Chhubche massif, then dips to the NE as it wraps around the northwestern margin of the Manaslu leucogranite. (**a**) Panoramic photograph of Chhubche (5605 m) from Chako. The near-2000-m-high vertical cliff displays, from bottom to top, the hornblende–biotite gneiss (Unit II) with thin interlayer of granitic augen gneiss (Unit III), micaceous marble (Unit IV), and garnet–biotite schist (Unit V) of the Greater Himalayan sequence. Note the pervasive leucogranitic injections within Units II and III. The Phu detachment is projected just above the massif, and is folded by the Chako antiform, which plunges shallowly (7°) to the NW. (**b**) Phu detachment (Pangla Ri fault) above village of Nar, with Oligocene-age north-verging folds affecting the Tethyan stratigraphy in the immediate hanging wall. (**c**) NW margin of the Manaslu leucogranite, as seen from the Pangre glacier, east of Phu.

### *Structural Level 2*

The intermediate structural level (Level 2) consists of upper-greenschist to lower-amphibolite facies garnet-bearing schist and gneiss, located in the hanging wall of the Chame detachment. Level 2 structures are characterized by a pervasive metamorphic foliation, overprinted by south-verging folds and related crenulation cleavage (Fig. 6a). Syntectonic garnets within Unit V indicate dominant southward rotation relative to cleavage during development of the metamorphic foliation (Gleeson & Godin 2006), consistent with moderately developed S-C fabrics and strain caps, which display evidence for general non-coaxial (mainly southward) ductile flow (Fig. 6b, c; cf. Passchier & Trouw 1996, p. 178). $D_2$ deformation is characterized by south-verging, asymmetric folds, and development of north-dipping axial planar cleavage ($S_2$) and hinge-parallel mineral lineations. The folds are open to closed, centimetre- to metre-scale and overturned to the south with shallowly NW-plunging fold hinges. Level 2 folds exhibit angular hinge zones and chevron fold shapes suggesting that they formed at higher structural levels than Level 1 folds of the same generation (Gleeson & Godin 2006).

### *Phu detachment*

In the Nar valley, Level 2 rocks are overlain by the Level 3 Tethyan sedimentary sequence along the Phu detachment (Searle & Godin 2003). The Phu detachment marks a clear metamorphic boundary between the Greater Himalayan sequence (*sensu stricto*) below, and the Tethyan sedimentary sequence above (Searle & Godin 2003). The immediate footwall rocks are dominated by intense flattening fabrics, mostly developed in the biotite marble Unit IV (Fig. 7a). In the northern end of the map area, in the Pangre glacier area, the northwestern part of the Manaslu leucogranite is cut by the Phu detachment (Searle & Godin 2003). In this area, the leucogranite contains a moderate solid-state foliation defined by muscovite

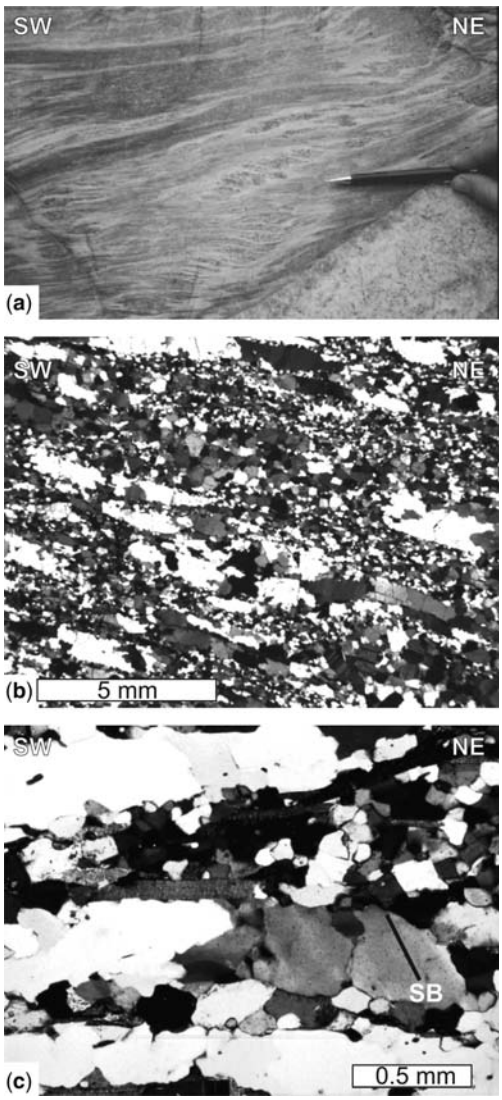


**Fig. 5.** Top-to-the-south ductile structures of Level 1. (**a**) Top-to-the-south hornblende–biotite mylonites within the Greater Himalayan sequence, Chako area. (**b**) Quartz proto-ribbon texture developed in the Unit III granitic augen gneiss (Sample N00-11b). (**c**) Detail of quartz subgrain boundaries (SB) in proto-ribbons. Their systematic north-dipping orientation is consistent with top-to-the-south ductile flow.

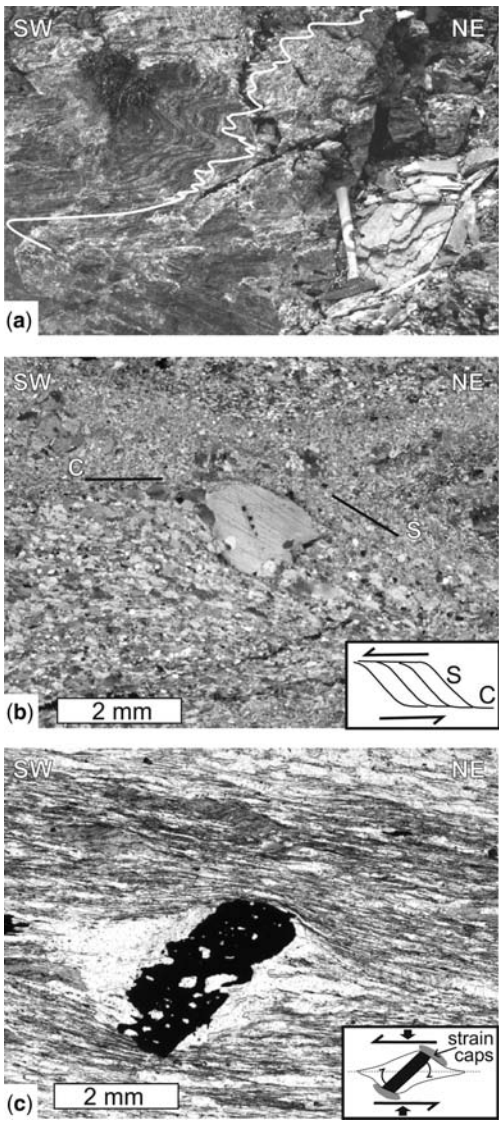


**Fig. 6.** Top-to-the-south ductile structures of Level 2. (**a**) South-verging folds and crenulations developed in the micaceous marble unit (Unit IV). Hammer is 40 cm long. (**b**) Moderately developed S-C fabric in Unit IV micaceous marble. Scale bar is 2 mm. (**c**) Opaque back-rotated grain (replaced equinoderm?) in Unit V, with asymmetric strain caps and pressure shadows indicating top-to-the-south general non-coaxial ductile flow. Scale bar is 2 mm.

and flattened dynamically recrystallized quartz (Fig. 7b). The immediate hanging wall of the Phu detachment is characterized by unmetamorphosed, yet highly deformed, Tethyan sedimentary rocks, which display numerous top-to-the-north brittle–ductile shear-sense indicators, such as sigma porphyroclasts and quarter structures (Fig. 7c; cf. Passchier & Trouw 1996). Cross-section constraints (see section A–A′, Fig. 3a) suggest the Phu detachment may cut the northern end of the Chame detachment, just north of Kyang (Figs 2 & 3a).

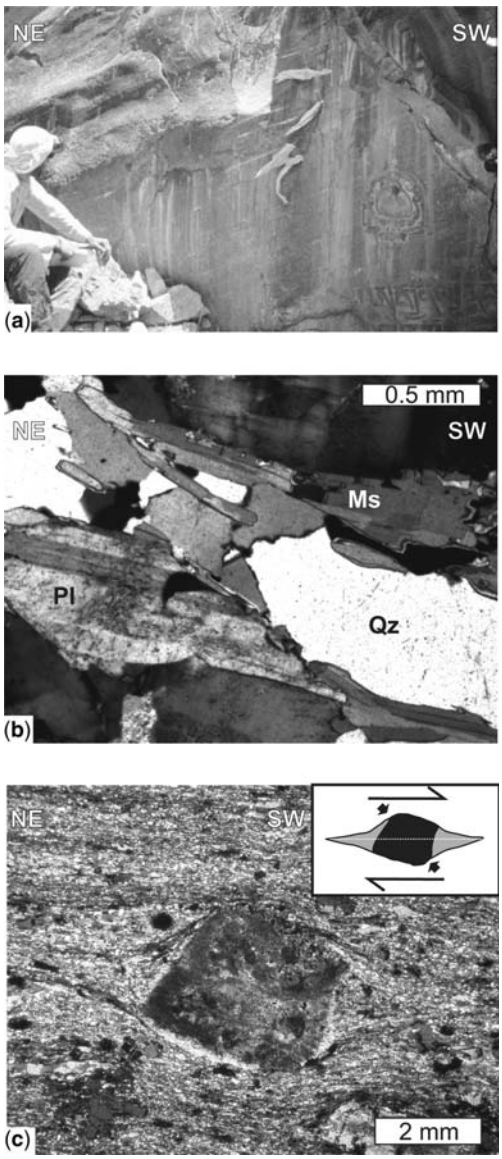


**Fig. 7.** Structures related to the Phu detachment. (**a**) Marble mylonite in the immediate footwall of the Phu detachment, between Kyang and Phu. (**b**) Photomicrograph of preferred alignment of muscovite and dynamically recrystallized quartz in the Manaslu leucogranite, in the immediate footwall of the Phu detachment, upper Pangre glacier (Sample N02-12). Ms, Muscovite; Pl, Plagioclase; Qz, Quartz. (**c**) Carbonate lithic porphyroclasts displaying sigma-type asymmetry and quarter structures developed in the shortening quadrants of the strain elipse (Passchier & Trouw 1996), compatible with top-to-the-north sense of shear in Triassic calcareous shale, in immediate hanging wall of Phu detachment, above Nar village (Sample N00-38).

### *Structural Level 3*

The structurally highest rocks of the Nar valley are the Level 3 Palaeozoic to Mesozoic rocks of the Tethyan sedimentary sequence, which lie in tectonic contact with Level 2 rocks. The deformation and metamorphic style of the Tethyan sedimentary sequence is quite distinct from the Greater Himalayan sequence. It is characterized by polyphase folding, and a very low degree of metamorphism, similar to the Tethyan sedimentary sequence in the Kali Gandaki valley, *c.* 35 km west (e.g. Godin 2003). The Tethyan sedimentary sequence is affected by three fold generations of contrasting vergence. The second-generation structures ($D_2$) are conspicuously defined by large-amplitude north-verging folds, interpreted to account for 150% vertical thickening of the Tethyan sedimentary sequence in Oligocene time, which are overprinted by south-verging kink folds and related crenulation cleavage ($D_4$; Godin 2003).

In the southern part of the map area, from Annapurna II to Chhubche, the Tethyan sedimentary sequence displays $D_2$ north-verging fold structures (Fig. 3a). The north side of the Annapurna–Lamjung face is characterized by a large-amplitude north-verging anticline, mostly developed in lower Palaeozoic strata of the Tethyan sedimentary sequence (Fig. 3a). This fold, termed the Annapurna–Nilgiri fold by Bordet *et al.* (1975), is part of a larger fold system (e.g. Godin 2003) that is possibly associated with a top-to-the-north (thrust?) fault juxtaposing Ordovician and Silurian rocks (Nilgiri and Sombre formations) above Triassic and Jurassic strata in the valley between Pisang peak and Nar village (Figs 3a & 4b). This possible thrust fault is interpreted to be associated with $D_2$ north-verging deformation, but alternatively could be an early top-to-the north STDS-related normal fault, subsequently flexed into a south-dipping orientation. Both this fault and the $D_2$ folds are cut by the Miocene Chame–Phu detachment system ($D_3$; Fig. 3a; Searle & Godin 2003).

North of Chhubche, on the northern limb of the Chako antiform, the structural style of the Tethyan sedimentary sequence is dominated by south-verging to upright folds, and shallow north-dipping top-to-the-south brittle–ductile thrust faults (Fig. 8). These structures are interpreted to be related to the south-verging $D_4$ structures observed further west in the Kali Gandaki valley (Godin 2003).

### *Crustal-scale buckling*

A series of megascopic folds buckle the Greater Himalayan sequence, the overlying Tethyan


**Fig. 8.** North-dipping, top-to-the-south minor thrusts in Triassic limestones, near Phu village. These structures are concentrated on the northern limb of the Chako antiform. Note circled tent for scale. The cliff in the foreground is approximately 15 m high.

sedimentary sequence, and all older structures including the Chame and Phu detachments (Fig. 3a; Searle & Godin 2003; Gleeson & Godin 2006). These buckles were previously described as the Mutsog synform and the Chako dome (Bordet *et al.* 1975; Coleman 1996), and are referred to here as the Mutsog synform and Chako antiform. The megascopic antiform–synform pair control outcrop patterns and foliation orientations in the Nar valley, and also account for the two sharp 90° bends in the surface trace of the STDS (Fig. 1a, b). The non-cylindrical buckles are upright and open with fold axes plunging shallowly NW. The amplitude (*c.* 4 km) and wavelength (*c.* 25 km) of the Mutsog synform–Chako antiform implies crustal-scale folding. These buckles are overprinted by south-verging structures within the Tethyan sedimentary sequence ($D_4$; Godin 2003).

## *Structural evolution*

The following structural evolution sequence is proposed based on field and microstructural observations, supported by regional correlations and previous studies (e.g. Godin 2003; Searle & Godin 2003; Schill *et al.* 2003; Gleeson & Godin 2006). The deformation phases follow the nomenclature of Godin (2003). The first folding phase ($D_1$) in the Palaeozoic rocks of the Kali Gandaki valley has not been observed in the Nar valley.

$D_2$ North-verging folds in the structural Level 3 Tethyan sedimentary sequence, and burial metamorphism of the Greater Himalayan sequence producing the metamorphic foliation in Levels 2 and 3. This episode is interpreted to occur at *c.* 35 Ma (Vannay & Hodges 1996; Godin *et al.* 2001; Godin 2003).

$D_3$ Southward extrusion of the Greater Himalayan sequence, producing top-to-the-south flow structures in Levels 2 and 3, accommodated by the STDS and the MCT. During extrusion, the Greater Himalayan sequence is progressively exhumed, and, at the current exposure level, the detachments evolve from ductile (Chame detachment) to brittle (Phu detachment) behaviour. The Manaslu leucogranite is emplaced in two phases (22 and 19 Ma; Guillot *et al.* 1994; Harrison *et al.* 1999), concomitant and slightly prior to motion on the Chame and Phu detachments, respectively. The Phu detachment has to be younger than 19 Ma, since it cuts the youngest intrusive phase of the Manaslu leucogranite (Searle & Godin 2003).

$D_{3-4}$ Large-amplitude buckling of the Greater Himalayan sequence, the STDS (Chame and Phu detachments), and the overlying Tethyan sedimentary sequence forming the Mutsog and Chako folds.

$D_4$ North-dipping, top-to-the-south-verging brittle–ductile thrust structures, and associated folds in the Tethyan sedimentary sequence, localized on the northern limb of the Chako antiform.

$D_5$ Localized north–south striking, steep brittle faults with minor offset and spaced brittle cleavage, associated with the onset of east–west extension at *c.* 14 Ma (Coleman & Hodges 1995).

## Timing constraints

### *U–Pb geochronology*

U–Pb geochronology was undertaken to: (1) assess the age of the granitic gneiss, and test the field interpretation that this unit is correlative with the Unit III Ordovician augen gneiss mapped further south in the Marsyandi and Kali Gandaki valleys (Coleman 1996; Godin *et al.* 2001); and (2) constrain the age of leucogranitic injections and deformation of the dykes within Level 1 rocks, as seen on the vertical east face of Chhubche (Fig. 4a). Although four samples were initially chosen for monazite and zircon analyses (see location on Figs 2 & 3a; results are presented in Table 1), only two samples (N-11b, N-22b) yielded reliable zircon results. Monazites were not recovered in any samples, most probably due to the predominance of calcareous rocks in the Nar valley that may have inhibited crystallization of monazite. Most of the analysed zircons contain very significant inheritance, except for fraction Z-1 in sample N-22b (concordant at $20.05 \pm 0.05$ Ma). Most of the inheritance is *c.* 470 Ma, which suggests the Nar metamorphic rocks are likely related to the uppermost part of the Greater Himalayan sequence (e.g. Godin *et al.* 2001).

Sample N-11b was collected from the granitic augen gneiss unit, at 4250 m elevation above Chako, on the east side of Nar Khola (Fig. 2). The sample was collected less than 1 m above a high-strain zone, defined by biotite schist (Fig. 9a). In thin section, the sample is dominated by quartz + plagioclase + biotite, and contains a strong foliation defined by proto-ribbon textures and preferred alignment of biotite (Fig. 5b, c). The quartz proto-ribbons contain dynamically recrystallized quartz with systematic north-dipping subgrain boundaries, consistent with other top-to-the-south shear-sense indicators visible in outcrop (Fig. 5a). The three zircon fractions analysed contain between three and eleven crystals with varying morphology including equant (Z-3) and flat (Z-2) grains and broken tips (Z-1) from crystals; our intention in selecting these fractions was to reduce or eliminate the influence of inherited cores. Inheritance is least likely in the flat grains and tips, and most likely in equant grains, which have the oldest $^{207}Pb/^{206}Pb$ age. Regression of the flat grains and tips yields an upper intercept age of $476.1 \pm 3.6$ Ma with a lower intercept of $29 \pm 34$ Ma. We interpret the upper intercept age as the protolith age (Fig. 9b).

Sample N-22b is from a boudinaged and folded 1.5-m-thick pegmatitic leucogranite dyke, injected in deformed hornblende–biotite gneisses (Fig. 2), visible on the cliffs north of Kyang (Fig. 9c). In thin section, the sample displays coarse (*c.* 1 mm) equigranular plagioclase + quartz + tourmaline + muscovite. The sample is not foliated, and does not contain any visible systematic array of subgrain boundaries. Four zircon analyses were produced, with between five and 14 crystals each, one of which (Z-1) produced a perfectly concordant abraded high-precision analysis with a concordia age of $20.05 \pm 0.06$ Ma, which is interpreted as the age of crystallization. All other fractions contained inherited zircons of a wide age range.

Analyses of two other samples were attempted: a weakly deformed tourmaline leucogranite dyke (N-6.4), and an undeformed quartz–feldspar porphyry (N-6) late dyke. This would have placed constraints on the minimum age of structures, but unfortunately every single analysis contained appreciable inheritance and no precise age information was obtained, though the data are presented in Table 1. The age of inherited zircons from N-6 appears to be $469 \pm 12$ Ma (lower intercept $21 \pm 39$ Ma), which is consistent with inheritance from the early Palaeozoic gneisses. The inheritance in sample N-6.4 is much more diverse and includes middle Proterozoic ages.

In summary, sample N-11b contains mainly mid-Ordovician zircons with either Pb-loss during Himalayan events, or thin overgrowths of the same age. This confirms that the augen gneiss is equivalent to Unit III exposed elsewhere in the Annapurna range (Hodges *et al.* 1996; Godin *et al.* 2001). The deformed leucogranitic dyke (N-22b) yielded a concordant *c.* 20 Ma zircon analysis, which is interpreted to represent the age of the melt, with some older zircons indicating a Proterozoic source, most probably inherited from the Greater Himalayan sequence into which the dyke was intruding.

### *$^{40}Ar/^{39}Ar$ thermochronology*

Twenty-three mineral separates from 15 samples were analysed by the $^{40}Ar/^{39}Ar$ method to constrain the youngest part of the tectonothermal history,

**Table 1.** *U–Pb isotopic data for zircons, Nar valley, Central Nepal*

| Analysis* | Weight (mg) | U (ppm) | Pb† (ppm) | $^{206}Pb/^{204}Pb$ | Pbc§ (pg) | Th†U | $^{206}Pb/^{283}U$¶ | 1 s.e. (%) | $^{207}Pb/^{235}U$¶ | 1 s.e. (%) | $^{207}Pb/^{206}Pb$¶ | 1 s.e. (%) | $^{206}Pb/^{238}U$¶ (Ma) | 2 s.e. (Ma) | $^{207}Pb/^{235}U$¶ (Ma) | 2 s.e. (Ma) | $^{207}Pb/^{206}Pb$§ (Ma) | 2 s.e. (Ma) | Correlation coefficient |
|---|---|---|---|---|---|---|---|---|---|---|---|---|---|---|---|---|---|---|---|
| *N-11b Granitic foliated augen gneiss (Unit III)* | | | | | | | | | | | | | | | | | | | |
| Z-1(4) tips | 0.0124 | 1088 | 68.64 | 7713 | 7 | 0.22 | 0.06514 | 0.27 | 0.5074 | 0.28 | 0.0565 | 0.067 | 406.8 | 2.1 | 416.7 | 1.9 | 472.2 | 3 | 0.97 |
| Z-2(3) flat | 0.028 | 912.7 | 66.8 | 7763 | 15 | 0.32 | 0.07362 | 0.15 | 0.5743 | 0.16 | 0.05658 | 0.06 | 457.9 | 1.3 | 460.8 | 1.2 | 475.1 | 2.6 | 0.93 |
| Z-3(11) eq | 0.1653 | 793.4 | 55.84 | 38060 | 16 | 0.22 | 0.07264 | 0.25 | 0.5695 | 0.26 | 0.05686 | 0.03 | 452 | 2.2 | 457.7 | 1.9 | 486.2 | 1.3 | 0.99 |
| *N-22b Deformed (boudinaged & folded) pegmatite* | | | | | | | | | | | | | | | | | | | |
| Z-1(5) r,c | 0.0043 | 6336 | 17.85 | 997 | 5 | 0.02 | 0.003116 | 0.14 | 0.019996 | 0.46 | 0.04654 | 0.42 | 20.05 | 0.05 | 20.1 | 0.18 | 25.9 | 20.1 | 0.43 |
| Z-2(7) r,c | 0.0135 | 4615 | 52.83 | 1819 | 25 | 0.17 | 0.01157 | 0.42 | 0.1543 | 0.43 | 0.09671 | 0.06 | 74.17 | 0.62 | 145.7 | 1.2 | 1561.7 | 2.2 | 0.99 |
| Z-3(11) r,c | 0.0121 | 5871 | 45.84 | 2467 | 14 | 0.14 | 0.008108 | 0.14 | 0.083258 | 0.17 | 0.07447 | 0.097 | 52.06 | 0.15 | 81.2 | 0.27 | 1054.3 | 3.9 | 0.82 |
| Z-4(14) r,c | 0.0096 | 6012 | 28.92 | 896 | 21 | 0.11 | 0.005119 | 0.15 | 0.040362 | 0.3 | 0.057188 | 0.24 | 32.91 | 0.1 | 40.18 | 0.24 | 498.8 | 10.5 | 0.62 |
| *N-6 Granitic foliated augen gneiss (Unit III)* | | | | | | | | | | | | | | | | | | | |
| Z-1(3) eq | 0.0262 | 1475 | 82.15 | 5237 | 26 | 0.26 | 0.05691 | 0.14 | 0.4416 | 0.16 | 0.05628 | 0.04 | 356.8 | 1 | 371.4 | 1 | 463.6 | 1.8 | 0.96 |
| Z-2(6) tips | 0.009 | 1500 | 77.85 | 4185 | 11 | 0.32 | 0.05214 | 0.15 | 0.4042 | 0.17 | 0.05622 | 0.08 | 327.7 | 1 | 344.7 | 1 | 461.1 | 3.5 | 0.88 |
| *N-6.4 Undeformed leucogranitic dyke* | | | | | | | | | | | | | | | | | | | |
| Z-1(11) r,c | 0.0318 | 1406 | 65.5 | 11450 | 12 | 0.2 | 0.04696 | 0.22 | 0.5871 | 0.23 | 0.09066 | 0.031 | 295.9 | 1.3 | 469 | 1.7 | 1439.5 | 1.2 | 0.99 |
| Z-2(11) r,c | 0.023 | 5164 | 51.18 | 454 | 171 | 0.28 | 0.01007 | 0.27 | 0.07626 | 0.43 | 0.0549 | 0.28 | 64.62 | 0.35 | 74.62 | 0.61 | 408.1 | 12.3 | 0.77 |
| Z-3(14) r,flat | 0.0172 | 5658 | 87.09 | 5776 | 16 | 0.23 | 0.015408 | 0.19 | 0.18756 | 0.2 | 0.088286 | 0.051 | 98.57 | 0.37 | 174.5 | 0.63 | 1388.7 | 2 | 0.97 |
| Z-4(3) r | 0.0156 | 13355 | 39.16 | 102 | 470 | 0.15 | 0.003074 | 0.7 | 0.026333 | 1.66 | 0.062137 | 1.3 | 19.78 | 0.28 | 26.39 | 0.86 | 678.8 | 55.1 | 0.68 |

*Z, zircon; all crystals were abraded; (1) refers to number of grains; r, rectangular; c, clear with no visible cores; eq, relatively equant; tips, tips broken off; flat, flat rectangular

†Atomic ratio of Th to U, calculated from $^{208}Pb/^{206}Pb$

‡Measured ratio, corrected for spike and Pb fractionation (0.13%/amu)

§Total common Pb in analysis, corrected for fractionation and spike

¶Corrected for blank Pb and U, and common Pb (Stacey-Kramers model Pb equivalent to interpreted age of mineral)

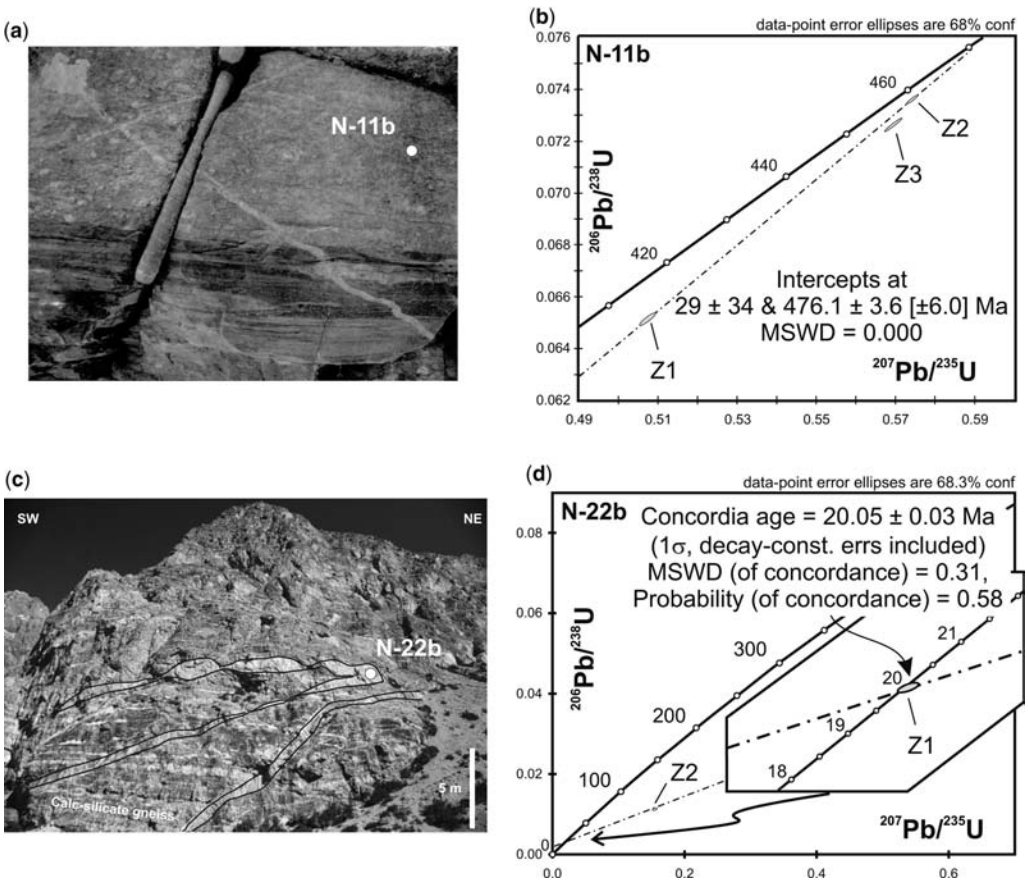


**Fig. 9.** U–Pb geochronology results from the Nar valley. (**a**) Field photograph of sample N-11b, showing the granitic augen gneiss, resting above its high-strain equivalent biotite schist. Hammer is 40 cm long. (**b**) Concordia plot of sample N-11b; the protolith age is best interpreted with a discordia line connecting fraction Z1 with Z2, yielding an upper intercept age of 476.1 $\pm$ 3.6 Ma. (**c**) Field photograph of sample site of N-22b, showing the folded and stretched nature of the leucogranitic dyke. (**d**) Concordia plot of sample N-22b; fraction Z1 yielded a concordant age of 20.05 $\pm$ 0.06 Ma.

and to complement the U–Pb data obtained in the Nar valley. Muscovite, biotite and hornblende mineral separates were selected to obtain a range of cooling ages with respect to the different isotopic closure temperatures of the respective minerals. Results (Table 2, Figs 3a & 10) are presented, interpreted and compared to published $^{40}Ar/^{39}Ar$ thermochronologic investigations in the Marsyandi area (e.g. Coleman & Hodges 1995, 1998), and in the Kali Gandaki area (Vannay & Hodges 1996; Godin *et al.* 2001).

The Th–Pb ion microprobe ages on monazites from the Manaslu leucogranite define two pulses of magmatism at 22.9 $\pm$ 0.6 Ma and 19.3 $\pm$ 0.3 Ma (Guillot *et al.* 1994; Harrison *et al.* 1999). Peak metamorphic conditions of the uppermost Greater Himalayan sequence (650°C; Gleeson & Godin 2006) are interpreted to have resulted from the Neohimalayan thermal pulse at 24–20 Ma (Coleman 1998; Godin *et al.* 2001), coeval with emplacement of the Manaslu leucogranite (*c.* 700–775°C; Guillot *et al.* 1994; Scaillet *et al.* 1995). The obtained $^{40}Ar/^{39}Ar$ ages are, for the most part, younger than 20 Ma, and therefore interpreted as cooling ages. The consistently small age differences between the Manaslu leucogranite, the leucogranitic dykes in the Nar (Sample N-22b at 20.05 $\pm$ 0.05 Ma), and the hornblende, biotite and muscovite ages require rapid cooling from >700°C to *c.* 300°C in less than 5 million years (*c.* 80°C/million years). For these rapid cooling rates,

**Table 2.** *Summary of $^{39}Ar/^{40}Ar$ results from the Nar valley*

| Sample | Rock unit | Mineral* | Plateau age† (Ma) ± 2σ | Total steps | % $^{39}$Ar (spectrum) | Isochron age† (Ma) ± 2σ | Isochron MSWD‡ |
|---|---|---|---|---|---|---|---|
| T-6 | Bt schist (Unit III) | Hbl | **24.9 ± 0.6**‡ | 6 | 91.8 | 24.8 ± 1.0 | 1.15 |
| N-38 | Pelitic schist (Unit V) | Hbl | **16.5 ± 0.6** | 8 | 95.3 | 16.9 ± 1.1 | 0.74 |
| N-40 | Augen gneiss (Unit III) | Ms | **16.9 ± 0.2** | 7 | 74.3 | 16.9 ± 0.4 | 0.58 |
| N-34 | Bt-Ms schist (Unit III) | Ms | **16.6 ± 0.4** | 9 | 97.7 | 16.7 ± 0.8 | 0.62 |
| L-9 | Marble (Unit IV) | Ms | **16.0 ± 1.3** | 7 | 94.1 | 16.1 ± 2.4 | 0.92 |
| T-21 | Marble (Unit IV) | Ms | N/A | N/A | N/A | **16.3 ± 2.5** | 0.61 |
| T-48 | Pelitic schist (Unit V) | Ms | **16.3 ± 0.5** | 6 | 71.9 | 12.7 ± 6.4 | 0.65 |
| T-134 | Pelitic schist (Unit V) | Ms | **16.3 ± 0.2** | 13 | 100 | 16.0 ± 0.6 | 0.72 |
| T-105 | Pelitic schist (Unit V) | Ms | **15.5 ± 0.5**§ | 5 | 89 | 15.8 ± 0.8 | 1.50 |
| N-102 | Pelitic schist (Unit V) | Ms | **14.8 ± 0.3** | 5 | 70.4 | 14.8 ± 1.0 | 1.40 |
| L-12 | Manaslu granite | Ms | **19.3 ± 0.2** | 13 | 100 | 19.0 ± 0.6 | 0.98 |
| T-141 | TSS | Ms | **15.9 ± 0.9** | 7 | 100 | 14.7 ± 6.1 | 1.30 |
| L-6 | Augen gneiss (Unit III) | Bt | **16.0 ± 0.3** | 9 | 96.3 | 15.7 ± 1.8 | 0.90 |
| T-6 | Bt schist (Unit III) | Bt | **16.6 ± 0.3** | 8 | 100 | 16.8 ± 0.7 | 1.17 |
| N-11 | Augen gneiss (Unit III) | Bt | **17.5 ± 0.3** | 8 | 80.5 | 17.9 ± 0.9 | 0.15 |
| N-34 | Bt schist (Unit III) | Bt | **16.1 ± 0.6** | 9 | 100 | 16.9 ± 2.0 | 2.00 |
| N-40 | Augen gneiss (Unit III) | Bt | **23.1 ± 0.1** | 8 | 82.1 | 23.1 ± 0.3 | 1.9 |
| L-9 | Marble (Unit IV) | Bt | **18.1 ± 0.2** | 7 | 83.5 | 18.3 ± 0.9 | 0.84 |
| T-48 | Pelitic schist (Unit V) | Bt | 18.2 ± 0.8 | 4 | 43.9 | 19.6 ± 1.9 | 0.35 |
| N-38 | Pelitic schist (Unit V) | Bt | **16.9 ± 0.6** | 7 | 90.5 | 16.0 ± 1.8 | 1.06 |
| T-134 | Pelitic schist (Unit V) | Bt | **16.1 ± 0.2** | 8 | 93.7 | 16.4 ± 0.9 | 0.48 |
| N-102 | Pelitic schist (Unit V) | Bt | **14.2 ± 0.3** | 9 | 100 | 14.3 ± 0.7 | 0.70 |
| T-105 | Pelitic schist (Unit V) | Bt | **14.3 ± 0.2** | 9 | 100 | 14.5 ± 0.7 | 1.20 |
| T-147 | TSS | Ms (WR) | 24.5 ± 0.7 | 5 | 76.2 | 24.8 ± 2.3 | 1.50 |

*Bt, biotite; Hbl, hornblende; Ms, muscovite
†Ages used in the interpretation are in bold
‡Mean square weighted deviation (MSWD) calculated following Roddick (1987)
§High temperature steps were lost in the initial run. Age reflects the plateau steps of the first run, combined with the second run results

we estimate closure temperatures based on published diffusion data as follows: hornblende 535 ± 50°C (Harrison 1981); muscovite 370 ± 50°C (Lister & Baldwin 1996); biotite 335 ± 50°C (Harrison *et al.* 1985; Grove & Harrison 1996).

## *Hornblende $^{40}Ar/^{39}Ar$ ages*

Two hornblende mineral fractions were analysed (T-6 and N-38). Sample T-6 is from the lowest exposed structural level (Level 1), in the core of the Chako antiform, structurally below the Chame detachment (Figs 2 & 3). The sample yielded a flat release spectrum with a plateau age of 24.9 ± 0.6 Ma, within error of the inverse isochron age (Table 2; Fig. 10). Sample N-38 was collected above the Chame detachment, in the immediate footwall of the overriding Phu detachment (Fig. 2). The obtained spectrum defines a plateau age of 16.5 ± 0.6 Ma, consistent with the inverse isochron age (Table 2; Fig. 10). Both samples have well-constrained, near-modern-day atmospheric $^{40}Ar/^{36}Ar$ ratios of 296 ± 11 and 288 ± 17 defined through regression analysis (modern atmosphere = 295.5), with MSWDs of 1.15 and 0.74, respectively (Table 2).

## *Muscovite $^{40}Ar/^{39}Ar$ ages*

A total of ten muscovite mineral factions were analysed. They were collected (Fig. 2) from Unit III augen gneiss (N-40) and highly strained equivalent biotite–muscovite schist (N-34), Unit IV (L-9, T-21) and Unit V (T-48, T-134, N-102, T-105). Two additional samples are from the Manaslu leucogranite (L-12), and from the Triassic unit of the Tethyan sedimentary sequence, in the immediate hanging wall of the Phu detachment above Nar village (T-141).

Both samples from Unit III, N-40 (granitic augen gneiss) and N-34 (highly sheared granitic gneiss), yield very good plateau ages of 16.9 ± 0.2 Ma and 16.6 ± 0.4 Ma, respectively (Fig. 10), and well-constrained initial atmospheric $^{40}Ar/^{36}Ar$ ratios (286 ± 51 and 293 ± 23, respectively; Table 2). Since their muscovite cooling ages are within error identical, the strain fabric responsible for the textural difference between samples N-40 and N-34 must therefore be older.

Samples from Unit IV (Ms-Bt marble) did not yield robust plateau ages. Sample L-9 yields a poorly constrained plateau age of 16.0 ± 1.3 Ma, with an initial atmospheric $^{40}Ar/^{36}Ar$ ratio of

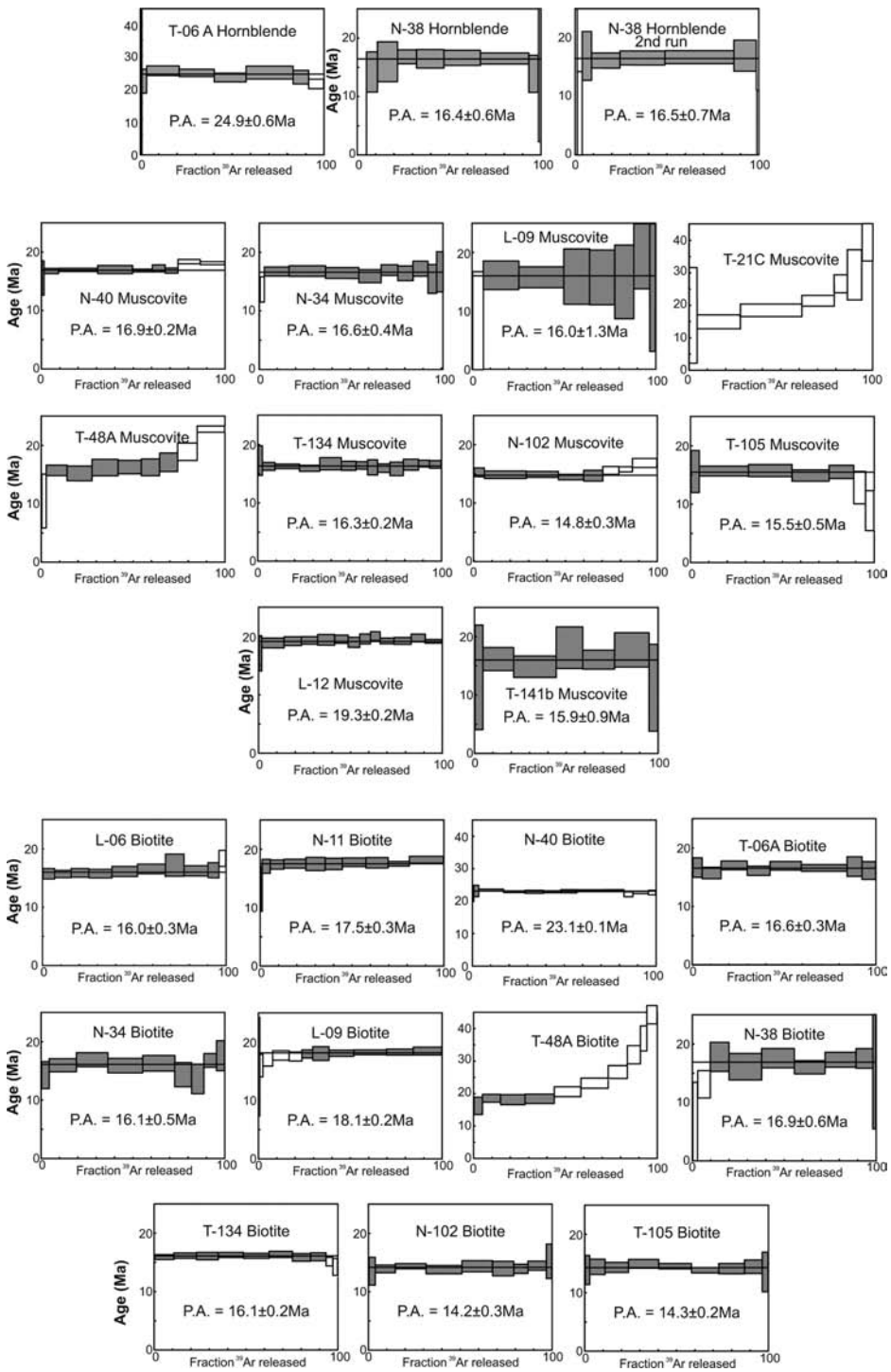


**Fig. 10.** $^{40}Ar/^{39}Ar$ release spectra diagrams of hornblende, muscovite and biotite samples used for thermochronology. The shaded steps within the release spectra indicate the increments used for calculating plateau ages. See text for explanation and discussion of data.

293 ± 22 (Table 2; Fig. 10). In contrast, sample T-21 did not yield a plateau age due to excess argon, as indicated by the high initial atmospheric $^{40}Ar/^{36}Ar$ ratio of 350 ± 23 (Table 2). By ignoring the low and high temperature steps, an inverse isochron age of 16.3 ± 2.5 Ma is obtained, consistent with the age of nearby samples. Both samples from Unit IV were collected on the northern limb of the Chako antiform, within a marble mylonite zone that displays significant top-to-the-south thrust shear-sense indicators.

Samples from Unit V (T-48, T-134, N-102, T-105) yielded muscovite cooling ages within error of each other. Sample T-48 has a good plateau age of 16.3 ± 0.5 Ma (with 72% of $^{39}Ar$), although the obtained inverse isochron age is poorly constrained with a high initial atmospheric $^{40}Ar/^{36}Ar$ ratio of 383 ± 160 (Table 2; Fig. 10). Samples T-134 and T-105 are from the northern and southern limbs of the Mutsog synform, respectively. Sample T-134 yielded a very robust 16.3 ± 0.2 Ma plateau age, in agreement with the inverse isochron age (initial atmospheric $^{40}Ar/^{36}Ar = 307 \pm 21$). Sample T-105 yielded a similar age, within error, to T-134, of 15.8 ± 1.5 Ma; however, some problems were encountered during the initial run, resulting in the loss of the higher-temperature steps. The interpreted age reflects the plateau steps of the first run, combined with the heating steps from the second run, plotted on the inverse isochron diagram (initial atmospheric $^{40}Ar/^{36}Ar = 276 \pm 20$; Table 2; Fig. 10). Both plateau and inverse isochron ages are in agreement, supporting this interpretation. Sample N-102 is from an intensely crenulated schist, located in the core of the Mutsog synform (Figs 2 & 3). A reliable plateau age of 14.8 ± 0.3 Ma was obtained, with a slight increase in age in the higher temperature steps (initial atmospheric $^{40}Ar/^{36}Ar = 295 \pm 61$; Table 2).

Sample L-12 is from the northeastern part of the Manaslu leucogranite (Fig. 2), on the south side of the Pangre glacier, in the immediate footwall of the Phu detachment (Searle & Godin 2003). The sample yielded a very robust plateau age of 19.3 ± 0.2 Ma, in agreement with the inverse isochron age (initial atmospheric $^{40}Ar/^{36}Ar = 311 \pm 32$; Table 2; Fig. 10). The obtained age is identical to monazite U–Th ages of the second pulse (Bimtang phase) of Manaslu magmatism at 19.3 ± 0.3 Ma (Harrison *et al.* 1999).

The last muscovite sample (T-141b) is from the immediate hanging wall of the Phu detachment, in shales of the Triassic Thini Formation, just above Nar village (Fig. 2). The sample yielded a plateau age of 15.9 ± 0.9 Ma, in agreement with the inverse isochron correlation diagram (initial atmospheric $^{40}Ar/^{36}Ar = 288 \pm 34$; Table 2; Fig. 10).

### *Biotite $^{40}Ar/^{39}Ar$ ages*

Eleven biotite samples were analysed. Five of these are from Unit III granitic augen gneiss (L-06, N-11 and N-40) and high-strain equivalent biotite schist (T-06 and N-34). Sample L-09 is from the marble mylonite zone just north of Kyang. The remaining five samples are from Unit V (T-48, N-38, T-134, N-102 and T-105). Since it is common for Himalayan biotites to contain unresolved excess argon (Roddick *et al.* 1980; McDougall & Harrison 1988), it was anticipated that the biotite samples would yield anomalously old age spectra compared to muscovite (e.g. Godin *et al.* 2001). However, although some biotite samples displayed anomalously old characteristics, most biotite ages are similar or younger than muscovite ages, with good plateau and inverse isochron correlation diagrams, supporting the quality of the data.

The three biotite samples from Unit III yield plateau ages of 23.1 ± 0.1 Ma (N-40), 17.5 ± 0.3 Ma (N-11) and 16.0 ± 0.3 Ma (L-06). Although all three results agree with their respective inverse isochron correlation diagrams (Table 2; Fig. 10), the age of the biotite in sample N-40 is distinctly older than muscovite in the same sample (16.9 ± 0.2 Ma), which suggests there might be unresolved excess argon. The result from sample N-11 is also slightly older than muscovites analysed from Unit III (see above), while sample L-06 yields a biotite age in agreement with muscovite results. We therefore cautiously disregard the results of N-40 and N-11. The two samples from the biotite schist yield flat release spectra with plateau ages of 16.6 ± 0.3 Ma (T-06) and 16.9 ± 0.6 Ma (N-34), in agreement with their inverse isochron ages (initial atmospheric $^{40}Ar/^{36}Ar = 286 \pm 23$ and 278 ± 32 for T-06 and N-34, respectively; Table 2; Fig. 10).

Sample L-09 yields a plateau (83.5% of $^{39}Ar$) age of 18.1 ± 0.2 Ma, coinciding with the inverse isochron age (initial atmospheric $^{40}Ar/^{36}Ar = 287 \pm 53$; Table 2; Fig. 10). However, muscovite analysis from the same sample yields an age 2 million years younger, suggesting this sample might also contain excess argon.

Four of the five pelite schist samples from Unit V yield very good plateau ages. The two southern samples yield young robust plateau ages (100% of $^{39}Ar$) of 14.2 ± 0.3 Ma (N-102) and 14.3 ± 0.2 Ma (T-105), in agreement with their inverse isochron ages (initial atmospheric $^{40}Ar/^{36}Ar$ ratio = 292 ± 32 and 284 ± 33 for N-102 and T-105, respectively; Table 2; Fig. 10). Samples N-38 and T-134 produced older good plateau ages of 16.9 ± 0.6 Ma (90.5% of $^{39}Ar$) and 16.1 ± 0.2 Ma (93.7% of $^{39}Ar$), respectively. Their initial atmospheric $^{40}Ar/^{36}Ar$ ratios are well-constrained

($310 \pm 29$ for sample N-38, and $277 \pm 51$ for sample T-134; Table 2; Fig. 10). Sample T-48 did not produce a reliable plateau or inverse isochron age (Table 2; Fig. 10). This sample contained significant excess argon, and is therefore discarded in our interpretations.

In summary, the Greater Himalayan sequence that crops out in the Nar valley yields hornblende ages ranging from 24.9 to 16.5 Ma, muscovite ages between 16.6 and 14.8 Ma, and biotite ages between 16.9 and 14.2 Ma. However, except for one *c.* 25 Ma hornblende and two *c.* 14 Ma biotite ages, all samples yield average ages systematically clustered around 16 Ma. We therefore interpret the $^{40}Ar/^{39}Ar$ ages to represent fairly homogeneous and rapid cooling of the Nar gneisses at *c.* 16 Ma.

## Discussion

### *Deformation features exposed in the Nar valley*

The data presented in this paper confirm that the Phu detachment footwall rocks correlate with the Greater Himalayan sequence. Units II and III are very similar to the Greater Himalayan sequence described further south in the Marsyandi and Kali Gandaki valleys, as well as in the Annapurna sanctuary (Coleman 1996; Hodges *et al.* 1996; Godin *et al.* 2001). Garnet–biotite thermometry on Unit V rocks indicates temperatures reached 650°C (upper-greenschist to amphibolite-facies metamorphism), confirming that the Chame detachment does not mark a metamorphic discontinuity at the top of the Greater Himalayan sequence (Gleeson & Godin 2006). Rather, it is a shear zone entirely positioned within the Greater Himalayan sequence, as suggested by Searle & Godin (2003). U–Pb geochronology of the Unit III granitic augen gneiss reveals a clear Ordovician origin, very similar to previously dated Unit III augen gneiss in the Kali Gandaki valley (*c.* 480 Ma; Godin *et al.* 2001). Structurally, the metamorphic rocks display penetrative top-to-the-south ductile flow structures, locally concentrated in high-strain zones, similar to Greater Himalayan sequence rocks exposed elsewhere in the Himalayan metamorphic core (Hodges *et al.* 1996; Vannay & Hodges 1996). Although structural Levels 1 and 2 are separated by the top-to-the-north Chame detachment, both levels are internally dominated by top-to-the-south ductile flow structures. During southward extrusion, the fault system was progressively exhumed, and the top-to-the-north detachment system evolved from ductile (Chame detachment) to brittle (Phu detachment) behaviour. The Phu detachment has to be younger than 19 Ma (Searle & Godin 2003), since it cuts the youngest intrusive phase of the Manaslu leucogranite dated at $19.3 \pm 0.3$ Ma (Harrison *et al.* 1999), and possibly the earlier Chame detachment. Motion on the Phu detachment was followed by large-amplitude buckling of the Greater Himalayan sequence, which folded the South Tibetan detachment system (Chame and Phu detachments), and the overlying Tethyan sedimentary sequence. The Mutsog and Chako folds are surface expressions of this event exposed in the Nar valley. Finally, renewed south-verging deformation created brittle–ductile thrust structures and associated folds in the Tethyan sedimentary sequence. We suggest that the northern limbs of the folded Greater Himalayan sequence provide natural ramps to localize these out-of-sequence thrusts.

### *Implications for cooling rate of the Greater Himalayan sequence*

Figure 11a shows three different cooling curves, established by compiling available ages from U–Pb geochronology obtained on zircon and monazite from melts, combined with $^{40}Ar/^{39}Ar$ cooling ages of hornblende, muscovite and biotite. In order to facilitate comparison, only samples collected from the upper levels of the Greater Himalayan sequence (Units II and higher) were considered.

The Kali Gandaki data are composed of U–Pb monazite ages, and hornblende, muscovite and biotite $^{40}Ar/^{39}Ar$ cooling ages (Vannay & Hodges 1996; Godin *et al.* 2001). They indicate a first thermal pulse at *c.* 35 Ma (Eohimalayan phase), interpreted to represent initial thickening following continental collision (Vannay & Hodges 1996; Godin *et al.* 2001). After a *c.* 15 million years isothermal period, the Greater Himalayan sequence underwent a second thermal pulse (Neohimalayan phase), coincident with sillimanite-grade metamorphism (Vannay & Hodges 1996; Godin *et al.* 2001). The Greater Himalayan sequence then cooled homogeneously, without any major structural disruption, through the muscovite cooling temperature between 15 and 13 Ma. The cooling part of the Kali Gandaki curve represents a cooling rate of *c.* 37°C/million years (Fig. 11a).

The Manaslu cooling curve combines Th–Pb ages of monazites from the Manaslu leucogranite (Harrison *et al.* 1999) with muscovite, biotite and alkali feldspar $^{40}Ar/^{39}Ar$ cooling ages (Copeland *et al.* 1990). Following emplacement of the youngest phase of the Manaslu leucogranite at *c.* 19.3 Ma (Harrison *et al.* 1999), the pluton cooled at a rate of *c.* 82°C/million years until *c.* 13.5 Ma (Copeland *et al.* 1990). The obtained cooling curve shows a

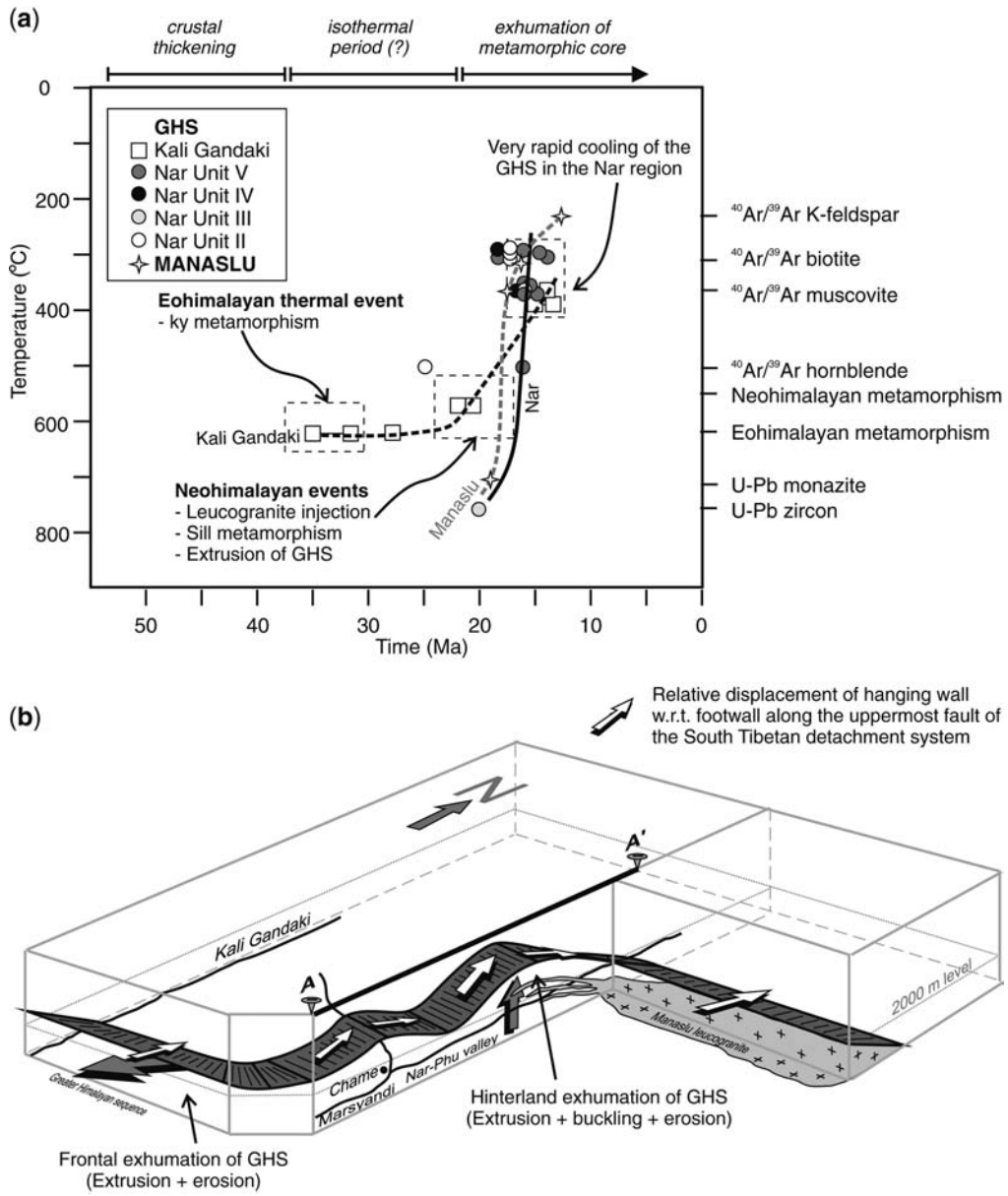


**Fig. 11.** (**a**) Temperature–time plot for the uppermost Greater Himalayan sequence (GHS) in the Nar valley. Kali Gandaki data from Vannay & Hodges (1996) and Godin *et al.* (2001); Manaslu data from Copeland *et al.* (1990) and Harrison *et al.* (1999). The temperature estimates for the Eohimalayan and the Neohimalayan events are taken from Vannay & Hodges (1996). See text for discussion. Ky, kyanite; Sill, sillimanite. (**b**) Schematic block diagram of present-day geometry of folded upper surface of the South Tibetan detachment system (Phu detachment), in relation to the Manaslu leucogranite.

faster period of exhumation (or unroofing) during the mid-Miocene, compared to the Greater Himalayan sequence in the Kali Gandaki (Fig. 11a).

The Nar cooling curve is obtained from compilation of the 24 hornblende, muscovite and biotite $^{40}Ar/^{39}Ar$ cooling ages presented in this paper, combined with the zircon age of sample N-22b. The upper part of the Greater Himalayan sequence in the Nar valley must have been at *c.* 750°C during crystallization of the leucogranitic dyke

(L-22b) at 20.05 Ma (Fig. 9d), and cooled through the biotite closure temperature ($335 \pm 50^{\circ}C$) at *c.* 16 Ma (Table 2). This represents a fast cooling rate of *c.* $80^{\circ}C$/million years, similar to the calculated cooling rate of the Manaslu leucogranite. However, the rapid cooling, and hence exhumation, of the Greater Himalayan sequence in the Nar valley occurred 2–3 million years prior to exhumation of equivalent structural-level rocks now exposed in the Kali Gandaki valley.

Figure 11b is a three-dimensional block diagram depicting the geometric relationships between the Manaslu leucogranite and the Greater Himalayan sequence of the Nar and Kali Gandaki valleys. The diagram also shows the folded nature of the upper strand of the STDS surface. In the Kali Gandaki valley, the STDS surface dips to the NE, then folds around the Annapurna massif into a series of synforms and antiforms, accounting for the northern step of its surface trace (Fig. 1a, b). The Kali Gandaki cooling data come from the 'frontal' previously well-described part of the Greater Himalayan sequence. The exhumation of the Greater Himalayan sequence in the Kali Gandaki is interpreted to be the result of tectonic denudation from top-to-the-north motion on the STDS, assisted by erosion of the south-facing side of the Annapurna Range. In contrast, the Greater Himalayan sequence in the Nar valley, exposed in the core of the Chako antiform, cooled 2–3 million years earlier, and at a faster rate, than the 'frontal' Kali Gandaki Greater Himalayan sequence. North-propagating tectonic denudation assisted by erosion would produce younger cooling ages towards the north. In contrast, the Greater Himalayan sequence in the Nar valley cooled before the frontal Kali Gandaki rocks. We propose that exhumation of the Nar valley rocks resulted from tectonic denudation associated with northward motion on the STDS, and assisted by buckling of the Greater Himalayan sequence shortly after normal-sense motion ceased on the Phu detachment. The Phu detachment cuts the youngest phase of the Manaslu leucogranite, and must therefore be younger than 19.3 Ma (Searle & Godin 2003). This buckling folded the Phu detachment, and probably initiated slightly prior to – or during – cooling at *c.* 16 Ma, which corresponds with the $^{40}Ar/^{39}Ar$ ages of most of the hornblende, muscovite and biotite in the Nar valley (Table 2). Buckling causing rapid exhumation is consistent with the fast cooling rates of the Manaslu leucogranite and the Greater Himalayan sequence in the Nar valley.

### *Implications for timing and mechanics of cessation of southward extrusion*

The Greater Himalayan sequence extruded southward during the Miocene along two opposite-sense shear-zone boundaries, the structurally lower MCT and structurally higher STDS (Hubbard & Harrison 1989; Searle & Rex 1989; Hodges *et al.* 1992, 1996). The geometry of this extrusion is commonly envisioned as either a 'channel' (Grujic *et al.* 2002; Beaumont *et al.* 2001) or a wedge (Burchfiel & Royden 1985; Hodges *et al.* 1992; Grujic *et al.* 1996; Grasemann *et al.* 1999). In both end-member geometries, the extrusion is possibly rendered feasible by Poiseuille-type flow in which the pressure gradient, induced by variation in crustal thickness at the southern edge of the Tibetan Plateau, produces highest velocities in the centre of the channel and opposite vorticity for the top and bottom of the channel (see review in Godin *et al.* 2006). Our thermochronology data indicate that folding of the Greater Himalayan sequence quickly followed cessation of motion along the upper extrusion boundary (Phu detachment), and is similar to data from Bhutan (Grujic *et al.* 2002). In central Nepal, the cessation of southward extrusion occurred between 19 and 16 Ma, prior to growth of the Lesser Himalayan duplex in late Miocene–Pliocene time (Robinson *et al.* 2003). This does not preclude the possibility that some segments of the MCT and/or STDS may have remained active after this time, as suggested by Harrison *et al.* (1997) and Hurtado *et al.* (2001); however, these younger fault motions are not related to synchronous and dynamically linked extrusion along the MCT–STDS couple (Godin *et al.* 2006).

Fold-and-thrust belts can be modelled in terms of a deforming wedge, propagating at a taper angle $\phi$ (Davis *et al.* 1983). In order to maintain a critical taper angle ($\phi_c$), changes in $\phi$ may instigate hinterland deformation (when $\phi < \phi_c$) or foreland deformation ($\phi > \phi_c$). The buckling of the Greater Himalayan sequence could therefore indicate a northward step in the Himalayan deformation, back-stepping away from the southward-propagating thrust system. Figure 12 portrays a suggested sequence of early to middle Miocene events that might have generated the geometry of structures observed in the Nar valley. We suggest that the hinterland, out-of-sequence buckling is controlled by a decrease in taper angle of the deforming wedge at the leading edge of the Himalayan deformation front (Fig. 12), a similar scenario to the dynamic compensation model proposed by Hodges *et al.* (1996).

It is suggested that rapid early extrusion during the coupled MCT–STDS phase in the early Miocene occurred at the critical taper angle ($\phi_c$), where the angle is maintained at equilibrium by southward ductile extrusion of mid-crustal material between the MCT and the lower strand of the STDS (Chame–Deurali–Annapurna detachment), balanced by frontal erosion on the southern slopes of the Himalaya (Fig. 12a).

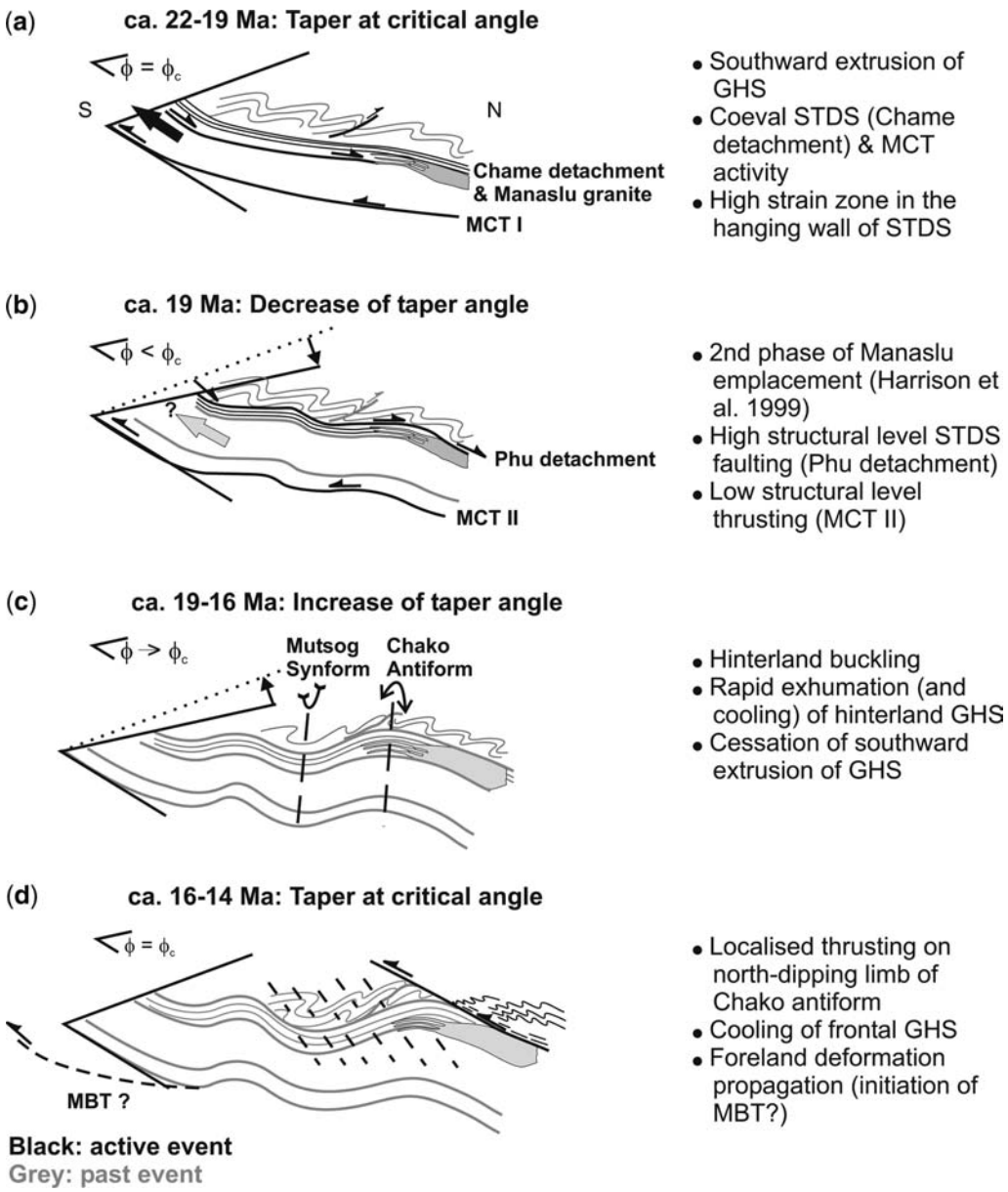


**Fig. 12.** Schematic evolution of the Greater Himalayan sequence (GHS) in the Nar valley and variation in the taper angle ($\phi$) of the deforming Himalayan wedge. (**a**) Early Miocene southward extrusion of the GHS by coeval motion along the Main Central thrust (MCT) and the ductile South Tibetan detachment system (STDS) fault (Chame detachment) at critical taper angle ($\phi_c$). (**b**) Decrease of the taper angle at *c.* 19 Ma, due to brittle activity along the structurally high Phu detachment, and sustained erosion on the southern deforming front of the Himalaya. (**c**) Increase and return to critical angle of the deforming taper by buckling the hinterland, favouring rapid exhumation of the GHS now exposed in the Nar valley. (**d**) Continued shortening generates and localizes top-to-the-south thrusts on the north-dipping limbs of the buckle folds. The return to critical angle of the deforming wedge favours foreland propagation, and development of the Main Boundary thrust (MBT) in mid-Miocene.

At *c.* 19 Ma, the angle of the deforming wedge decreased and slip in the STDS migrated structurally higher from the Chame detachment to the Phu detachment, as the Greater Himalayan sequence extruded and cooled (Fig. 12b). The decrease in angle may have resulted from continued activity along the ductile–brittle strand of the STDS (Phu detachment), while MCT motion ceased. Alternatively, the decrease in angle of the deforming wedge may have resulted from a combination of slowing extrusive flow rates and/or an increase in erosion. The $^{87}Sr/^{86}Sr$ ratio in marine carbonate sediments dramatically increases at *c.* 18 Ma, which is interpreted to represent a sharp increase in weathering denudation rates in the Himalaya (Richter *et al.* 1992), and may be related to strengthening of the Indian Monsoon (Raymo & Ruddiman 1992; Molnar *et al.* 1993). If continued activity along the brittle strand of the STDS (Phu detachment) persisted while motion on the MCT ceased, this would imply that the younger normal-sense fault motion resulted in true horizontal extension. This would also imply that motion along the different strands of the STDS may have different causes. Although the lower ductile strand (Chame detachment) may be linked to footwall extrusion of the Greater Himalayan sequence beneath a 'fixed' Tethyan sedimentary sequence, the upper, younger and brittle strand could be linked to 'true' extension, associated with far-field critical taper adjustments.

Between 19 and 16 Ma, top-to-the north normal motion along the Phu detachment ceased, and the Greater Himalayan sequence in the Nar valley was buckled. The Chako antiform, combined with subsequent valley incision, forms an apparent structural window in the Greater Himalayan sequence. The 'hinterland' buckling accelerated exhumation of the Manaslu leucogranite and the Greater Himalayan sequence now exposed in the Nar valley, and contributed to an increase of the taper angle (Fig. 12c).

Continued shortening between 16 and 14 Ma localized renewed top-to-the-south thrusting on the north-dipping limbs of the folded Greater Himalayan sequence, locally reactivating as thrust faults older top-to-the-north (previously normal-sense motion) fault segments, such as the Phu detachment (Fig. 12d). This late thrusting must have occurred after folding of the Greater Himalayan sequence, but before onset of east–west brittle extension at *c.* 14 Ma, as documented in the Marsyandi valley (Coleman & Hodges 1995).

## Conclusion

We suggest that ductile extrusion of the Greater Himalayan sequence occurred at *c.* 25–19 Ma above the ductile (structurally higher) MCT and below the ductile strand of the STDS (Chame detachment). Peak temperatures were attained within the Greater Himalayan sequence from *c.* 35 Ma, and temperatures remained high until the end of crustal melting that generated the Manaslu leucogranite and the Chako dyke network at *c.* 20 Ma.

Structural cross-cutting relationships, regional cross-sections and restoration, and metamorphic petrology indicate that southward extrusion of the Greater Himalayan sequence terminated with cessation of normal-sense motion on the brittle upper strand of the STDS, the Phu detachment, at *c.* 19 Ma. This was followed almost immediately by crustal-scale buckling, resulting in rapid cooling of the Greater Himalayan sequence now exposed in the metamorphic culmination of the Nar valley. The thermochronology of samples from the the Nar valley indicates that cooling occurred very rapidly, 2–3 million years earlier than in the frontal part of the extruding Greater Himalayan sequence. Although extrusion in the frontal part of the slab must have locked at the same time as in the Nar valley, the exhumation and cooling of the gneisses was slower, most probably assisted only by erosion, rather than by rapid folding as in the case in the Nar valley samples. This buckling also indicates a step northward in deformation of the Himalayan belt, which may be a response to a lower taper geometry in the foreland due to the erosion that might have initiated and driven extrusion in the first place.

Invaluable field assistance was provided by C. Olsen, N. Portelance and P. Tamang and his friendly crew. Funding from a Natural Science and Engineering Research Council of Canada operating grant and graduate scholarship to L.G. and T.G., respectively, and a Natural Environment Research Council grant to M.S. are gratefully acknowledged. Many ideas expressed in this paper benefited from discussions with R. Brown, D. Kellett and K. Larson. The first expedition to the Nar valley in 2000 was made possible by a Natural Science and Engineering Research Council of Canada operating grant to R. Brown, of Carleton University. Reviewers M. Hubbard, S. Guillot and editor R. Law are thanked for constructive comments on an earlier draft of this manuscript.

This paper is dedicated to the memory of Pasang Tamang (1960–2005).

## References

ARITA, K. 1983. Origin of the inverted metamorphism of the lower Himalayas, central Nepal. *Tectonophysics*, **95**, 43–60.

BEAUMONT, C., JAMIESON, R. A., NGUYEN, M. H. & LEE, B. 2001. Himalayan tectonics explained by extrusion of a low-viscosity crustal channel coupled to focused surface denudation. *Nature*, **414**, 738–742.

BEAUMONT, C., JAMIESON, R. A., NGUYEN, M. H. & MEDVEDEV, S. 2004. Crustal channel flows: 1. Numerical models with applications to the tectonics of the Himalayan–Tibetan orogen. *Journal of Geophysical Research*, **109**. DOI: 10.1029/2003JB002809.

BORDET, P., COLCHEN, M., KRUMMENACHER, D., LE FORT, P., MOUTERDE, R. & REMY, M. 1971. *Recherches géologiques dans l'Himalaya du Népal: région de la Thakhola*. Centre de la Recherche Scientifique, Paris.

BORDET, P., COLCHEN, M. & LE FORT, P. 1975. *Recherches géologiques dans l'Himalaya du Népal: région du Nyi-Shang*. Centre de la Recherche Scientifique, Paris.

BOUCHEZ, J.-L. & PÊCHER, A. 1976. Plasticité du quartz et sens de cisaillement dans les quartzites du Grand Chevauchement Central Himalayen. *Bulletin de la Société Géologique de France*, **18**, 1377–1385.

BROWN, R. L. & NAZARCHUK, J. H. 1993. Annapurna detachment fault in the Greater Himalaya of central Nepal. *In*: TRELOAR, P. J. & SEARLE, M. P. (eds) *Himalayan Tectonics*. Geological Society, London, Special Publications, **74**, 461–473.

BRUNEL, M. 1986. Ductile thrusting in the Himalayas: shear sense criteria and stretching lineations. *Tectonics*, **5**, 247–265.

BURCHFIEL, B. C. & ROYDEN, L. H. 1985. North–south extension within the convergent Himalayan region. *Geology*, **13**, 679–682.

BURCHFIEL, B. C., CHEN, Z., HODGES, K. V., LIU, Y., ROYDEN, L. H., DENG, C. & XU, J. 1992. *The South Tibetan Detachment System, Himalaya Orogen: Extension contemporaneous with and parallel to shortening in a collisional mountain belt*. Geological Society of America, Special Paper, **269**.

BURG, J.-P. 1983. *Carte Géologique du sud du Tibet*. Ministry of Geology Peking and Centre National de Recherche Scientifique, Paris.

CABY, R., PÊCHER, A. & LE FORT, P. 1983. Le grand chevauchement central himalayen: nouvelles données sur le métamorphisme inverse à la base de la Dalle du Tibet. *Revue de Géologie Dynamique et de Géographie Physique*, **24**(2), 89–100.

CATLOS, E. J., HARRISON, T. M., MANNING, C. E., GROVE, M., RAI, S. M., HUBBARD, M. S. & UPRETI, B. N. 2002. Records of the evolution of the Himalayan orogen from in situ Th-Pb ion microprobe dating of monazite: eastern Nepal and western Garhwal. *Journal of Asian Earth Sciences*, **20**, 459–479.

COLCHEN, M., LE FORT, P. & PÊCHER, A. 1981. Geological map of the Annapurnas-Manaslu-Ganesh Himalaya of Nepal. *In*: GUPTA, H. K. & DELANY, F. M. (eds). *Zagros – Hindu Kush – Himalaya: A Geodynamic Evolution*. American Geophysical Union, Geodynamics Series 3, Map scale 1:200,000.

COLCHEN, M., Le FORT, P. & PÊCHER, A. 1986. *Recherches géologiques dans l'Himalaya du Népal: Annapurna – Manaslu – Ganesh Himal*. Éditions du centre National de la Recherche Scientifique, Paris.

COLEMAN, M. E. 1996. Orogen-parallel and orogen-perpendicular extension in the central Nepalese Himalayas. *Geological Society of America Bulletin*, **108**, 1594–1607.

COLEMAN, M. E. 1998. U-Pb constraints on Oligocene–Miocene deformation and anatexis within the central Himalaya, Marsyandi valley, Nepal. *American Journal of Science*, **298**, 553–571.

COLEMAN, M. E. & HODGES, K. V. 1995. Evidence for Tibetan plateau uplift before 14 Myr ago from a new minimum age for east-west extension. *Nature*, **374**, 49–52.

COLEMAN, M. E. & HODGES, K. V. 1998. Contrasting Oligocene and Miocene thermal histories from the hanging wall and footwall of the South Tibetan detachment in the central Himalaya from 40Ar/39Ar thermochronology, Marsyandi valley, central Nepal. *Tectonics*, **17**, 726–740.

COPELAND, P., HARRISON, T. M. & LE FORT, P. 1990. Age and cooling history of the Manaslu granite: implication for Himalayan tectonics. *Journal of Volcanology and Geothermal Research*, **44**, 33–50.

DAVIS, D., SUPPE, J. & DAHLEN, F. A. 1983. Mechanics of fold-and-thrust belts and accretionary wedges. *Journal of Geophysical Research*, **88**, 1153–1172.

FUCHS, G., WIDDER, R. W. & TULADHAR, R. 1988. Contributions to the geology of the Annapurna range (Manang, area, Nepal). *Jahrbuch der Geologischen Bundesanstalt*, *Wien*, **131**, 593–607.

FUCHS, G., REGMI, K. & SCHILL, E. 1999. Note on the geology of the Nar – Manag region in northern Nepal (Himalaya). Abstract volume, 14th Himalaya–Karakorum–Tibet workshop, Kloster Ettal. *Terra Nostra*, **2**, 46–47.

GARZANTI, E. 1999. Stratigraphy and sedimentary history of the Nepal Tethys Himalaya passive margin. *Journal of Asian Earth Sciences*, **17**, 805–827.

GARZANTI, E., GORZA, M., MARTELLINI, L. & NICORA, A. 1994. Transition from diagenesis to metamorphism in the Paleozoic to Mesozoic succession of the Dolpo-Manang Synclinorium and Thakkhola graben (Nepal Tethys Himalaya). *Eclogae Geologicae Helvetica*, **87**, 13–632.

GLEESON, T. & GODIN, L. 2006. The Chako antiform: a folded segment of the Greater Himalayan sequence, Nar valley, Central Nepal Himalaya. *Journal of Asian Earth Sciences*, **27**, 717–734.

GODIN, L. 2001. The Chako dome: an enigmatic structure in the hanging wall of the South Tibetan detachment, Nar valley, central Nepal. *Journal of Asian Earth Sciences*, **19**, 22–23.

GODIN, L. 2003. Structural evolution of the Tethyan sedimentary sequence, central Nepal Himalaya. *Journal of Asian Earth Sciences*, **22**, 307–328.

GODIN, L., BROWN, R. L. & HANMER, S. 1999. High strain zone in the hanging wall of the Annapurna detachment, central Nepal Himalaya. *In*: MACFARLANE, A. M., SORKHABI, R. & QUADE, J. (eds) *Himalaya and Tibet: Mountain Roots to Mountain Tops*. Geological Society of America, Special Paper **328**, 199–210.

GODIN, L., PARRISH, R. R., BROWN, R. L. & HODGES, K. 2001. Crustal thickening leading to exhumation of the metamorphic core of the central Nepal Himalaya: Insight from U-Pb geochronology and $^{40}Ar/^{39}Ar$ thermochronology. *Tectonics*, **20**, 729–747.

GODIN, L., GRUJIC, D., LAW, R. D. & SEARLE, M. P. 2006. Channel flow, ductile extrusion and exhumation in continental collision zones: an introduction. *In*: LAW, R. D., SEARLE, M. P. & GODIN, L. (eds) *Channel Flow, Ductile Extrusion, and Exhumation in Continental Collision Zones.* Geological Society, London, Special Publications, **268**, 1–23.

GRADSTEIN, F. M., VON RAD, U., GIBLING, M. R. *ET AL.* 1992. The Mesozoic continental margin of central Nepal. *Geologisches Jahrbuch*, **77**.

GRASEMANN, B., FRITZ, H. & VANNAY, J.-C. 1999. Quantitative kinematic flow analysis from the Main Central thrust zone (NW-Himalaya, India): implications for a decelerating strain path and the extrusion of orogenic wedges. *Journal of Structural Geology*, **21**, 837–853.

GROVE, M. & HARRISON, T. M. 1996. $^{40}Ar$ diffusion in Fe-rich biotite. *American Mineralogist*, **81**, 940–951.

GRUJIC, D., CASEY, M., DAVIDSON, C., HOLLISTER, L. S., KÜNDIC, R., PAVLIS, T. & SCHMID, S. 1996. Ductile extension of the Higher Himalayan Crystalline in Bhutan: evidence from quartz microfabrics. *Tectonophysics*, **260**, 21–43.

GRUJIC, D., HOLLISTER, L. S. & PARRISH, R. R. 2002. Himalayan metamorphic sequence as an orogenic channel: insight from Bhutan. *Earth and Planetary Science Letters*, **198**, 177–191.

GUILLOT, S., PÊCHER, A., ROCHETTE, P. & LE FORT, P. 1993. The emplacement of the Manaslu granite of Central Nepal: field and and magnetic susceptibility constraints. *In*: TRELOAR, P. J. & SEARLE, M. P. (eds) *Himalayan Tectonics*. Geological Society, London, Special Publications, **74**, 413–428.

GUILLOT, S., HODGES, K., LE FORT, P. & PÊCHER, A. 1994. New constraints on the age of the Manaslu leucogranite: evidence for episodic tectonic denudation in the central Himalayas. *Geology*, **22**, 559–562.

HARRISON, T. M. 1981. Diffusion of $^{40}Ar$ in hornblende. *Contributions to Mineralogy and Petrology*, **78**, 324–331.

HARRISON, T. M., DUNCAN, I. & MCDOUGALL, I. 1985. Diffusion of $^{40}Ar$ in biotite: Temperature, pressure and compositional effects. *Geochimica et Cosmochimica Acta*, **49**, 2461–2468.

HARRISON, T. M., RYERSON, F. J., LE FORT, P., YIN, A., LOVERA, O. M. & CATLOS, E. J. 1997. A late Miocene–Pliocene origin for the Central Himalayan inverted metamorphism. *Earth and Planetary Science Letters*, **146**, E1–E7.

HARRISON, T. M., GROVE, M., MCKEEGAN, K. D., COATH, C. D., LOVERA, O. M. & LE FORT, P. 1999. Origin and episodic emplacement of the Manaslu intrusive complex, central Himalaya. *Journal of Petrology*, **40**, 3–19.

HODGES, K. V. 2000. Tectonics of the Himalaya and southern Tibet from two perspectives. *Geological Society of America Bulletin*, **112**, 324–350.

HODGES, K. V., PARRISH, R. R., HOUSH, T. B., LUX, D. R., BURCHFIEL, B. C., ROYDEN, L. H. & CHEN, Z. 1992. Simultaneous Miocene extension and shortening in the Himalayan orogen. *Science*, **258**, 1466–1470.

HODGES, K. V., PARRISH, R. R. & SEARLE, M. P. 1996. Tectonic evolution of the central Annapurna Range, Nepalese Himalayas. *Tectonics*, **15**, 1264–1291.

HUBBARD, M. S. & HARRISON, T. M. 1989. $^{40}Ar/^{39}Ar$ age constraints on deformation and metamorphism in the Main Central Thrust Zone and Tibetan Slab, eastern Nepal Himalaya. *Tectonics*, **8**, 865–880.

HURTADO Jr, J. M., HODGES, K. V. & WHIPPLE, K. X. 2001. Neotectonics of the Thakkhola graben and implications for recent activity on the South Tibetan fault system in the central Nepal Himalaya. *Geological Society of America Bulletin*, **113**, 222–240.

LE FORT, P. 1975. Himalayas: the collided range. Present knowledge of the continental arc. *American Journal of Science*, **275-A**, 1–44.

LE FORT, P. 1981. Manaslu leucogranite: a collision signature of the Himalaya – A model for its genesis and emplacement. *Journal of Geophysical Research*, **86**, 545–568.

LE FORT, P., PÊCHER, A. & UPRETI, B. N. 1986. A section through the Tibetan Slab in central Nepal (Kali Gandaki valley): mineral chemistry and thermobarometry of the Main Central thrust zone. *Science de la Terre, Mémoire* **47**, 211–228.

LE FORT, P., GUILLOT, S. & PÊCHER, A. 1999. Une carte géologique de l'Himlung Himal, massif du Manaslu. *La Montagne et Alpinisme*, **95**, 22–27.

LISTER, G. S. & BALDWIN, S. L. 1996. Modelling the effect of arbitrary P-T-t histories on argon diffusion in minerals using the MacArgon program for the Apple Macintosh. *Tectonophysics*, **253**, 83–109.

MCDOUGALL, I. & HARRISON, T. M. 1988. *Geochronology and Thermochronology by the $^{40}Ar/^{39}Ar$ Method*. Oxford University Press, New York.

MOLNAR, P., ENGLAND, P. & MARTINOD, J. 1993. Mantle dynamics, uplift of the Tibetan Plateau, and the indian monsoon. *Reviews in Geophysics*, **31**, 357–396.

MURPHY, M. A. & HARRISON, T. M. 1999. Relationship between leucogranites and the Qomolangma detachment in the Rongbuk Valley, south Tibet. *Geology* **27**, 831–834.

PASSCHIER, C. W. & TROUW, R. A. J. 1996. *Microtectonics*. Springer-Verlag, Berlin.

PÊCHER, A. 1975. The Main Central Thrust of the Nepal Himalaya and the related metamorphism in the Modi-Khola cross-section (Annapurna range). *Himalayan Geology*, **5**, 115–131.

PÊCHER, A. 1991. The contact between the Higher Himalaya crystallines and the Tibetan sedimentary series: Miocene large-scale dextral shearing. *Tectonics*, **10**, 587–598.

RAYMO, M. E. & RUDDIMAN, W. F. 1992. Tectonic forcing of Late Cenozoic climate. *Nature*, **359**, 117–122.

RICHTER, F. M., ROWLEY, D. B. & DE PAOLO, D. J. 1992. Sr isotope evolution of seawater – the role of tectonics. *Earth and Planetary Science Letters*, **109**, 11–23.

ROBINSON, D. M., DECELLES, P. G., GARZIONE, C. N., PEARSON, O. N., HARRISON, T. M., & CATLOS, E. J. 2003. Kinematic model for the Main Central thrust in Nepal. *Geology*, **31**, 359–362.

RODDICK, J. C. 1987. Generalized numerical error analysis with applications to geochronology and thermodynamics. *Geochimica et Cosmochimica Acta*, **51**, 2129–2135.

RODDICK, J. C., CLIFF, R. A. & REX, D. C. 1980. The evolution of excess argon in Alpine biotites – A $^{40}Ar/^{39}Ar$ analysis. *Earth and Planetary Science Letters*, **48**, 185–208.

ROYDEN, L. H. 1996. Coupling and decoupling of crust and mantle in convergent orogens: implications for strain partitioning in the crust. *Journal of Geophysical Research*, **101**, 17679–17705.

SCAILLET, B., PÊCHER, A., ROCHETTE, P. & CHAMPENOIS, M. 1995. The Gangotri granite (Garhwal Himalaya): Laccolithic emplacement in an extending collisional belt. *Journal of Geophysical Research*, **100**, 585–607.

SCHILL, E., APPEL, E., GODIN, L., CROUZET, C., GAUTAM, P. & REGMI, K. 2003. Record of deformation by AMS and secondary inclinations in the Nar/Phu valley (central Nepal). *Tectonophysics*, **377**, 197–209.

SCHNEIDER, C. & MASCH, L. 1993. The metamorphism of the Tibetan Series from the Manang area, Marsyandi valley, central Nepal. *In*: TRELOAR, P. J. & SEARLE, M. P. (eds) *Himalayan Tectonics.* Geological Society, London, Special Publications, **74**, 357–374.

SEARLE, M. P. & GODIN, L. 2003. The South Tibetan detachment system and the Manaslu leucogranite: a structural reinterpretation and restoration of the Annapurna – Manaslu Himalaya, Nepal. *Journal of Geology*, **111**, 505–524.

SEARLE, M. P. & REX, A. J. 1989. Thermal model for the Zanskar Himalaya. *Journal of Metamorphic Geology*, **7**, 127–134.

SEARLE, M. P., PARRISH, R. P., HODGES, K. V., HURFORD, A., AYRES, M. W. & WHITEHOUSE, M. J. 1997. Shisha Pangma leucogranite, South Tibetan Himalaya: Field relations, geochemistry, age, origin, and emplacement. *Journal of Geology*, **105**, 295–317.

SEARLE, M. P., SIMPSON, R. L., LAW, R. D., PARRISH, R. R. & WATERS, D. J. 2003. The structural geometry, metamorphic and magmatic evolution of the Everest massif, High Himalaya of Nepal – South Tibet. *Journal of the Geological Society*, London, **160**, 345–366.

VANNAY, J.-C. & GRASEMANN, B. 2001. Himalayan inverted metamorphism and syn-convergence extension as a consequence of a general shear extrusion. *Geological Magazine*, **138**, 253–276.

VANNAY, J.-C. & HODGES, K. V. 1996. Tectonometamorphic evolution of the Himalayan metamorphic core between the Annapurna and Dhaulagiri, central Nepal. *Journal of Metamorphic Geology*, **14**, 635–656.

VIDAL, P., COCHERIE, A. & LE FORT, P. 1982. Geochemical investigations of the origin of the Manaslu leucogranite (Himalaya, Nepal). *Geochimica et Cosmochimica Acta*, **46**, 2279–2292.

WEISMAYR, G. & GRASEMANN, B. 2002. Eohimalayan fold and thrust belt: Implications for the geodynamic evolution of the NW-Himalaya (India). *Tectonics*, **21**, 1058. DOI: 10/1029/2002TC001363.

YIN, A. 2003. Reinterpreting the South Tibet Detachment as a passive roof fault in a large scale fault-bend fold system during Miocene evolution of the Himalayas. *Abstract volume, 18th Himalaya–Karakorum–Tibet workshop*, Monte Verita, Switzerland, 131.